Challenge Journal of Concrete Research Letters

Research Article

Predicting compressive strength of heavyweight concrete using deep neural networks and Box–Behnken design

Amir Hossein Derakhshan Nezhad [a], Seayf Allah Hemati [a,*], Omid Rezaifar [a]

[a] *Department of Civil Engineering, Semnan University, 35131-19111 Semnan, Iran*

ABSTRACT

This study investigates the prediction and evaluation of compressive strength in heavyweight concrete incorporating magnetite and steel slag, using two advanced modeling techniques: Deep Artificial Neural Networks (DANN) and Box-Behnken Response Surface Methodology (BBRSM). A total of 324 concrete specimens were prepared based on 36 unique mix designs. Non-destructive testing methods ultrasonic pulse velocity (UPV) and Schmidt rebound hammer (SRH) were employed to characterize material properties. The 28-day compressive strength of each sample was determined following ASTM C39 standards. Data from UPV and SRH tests, along with mix parameters such as the water-cement ratio, were used as inputs for both models. The DANN model, developed using a hybrid architecture combining Convolutional Neural Network (CNN) and Long Short-Term Memory (LSTM), achieved superior predictive performance, with a coefficient of determination (R^2) of 0.9951 and a root mean square error (RMSE) of 0.0314 MPa. This corresponds to a coefficient of variation of just 0.045%, with a standard deviation error of 0.02% relative to the mean compressive strength of approximately 70 MPa. In contrast, the BBRSM model, employing a sixth-degree polynomial equation, yielded an R^2 of 0.9628 and a standard deviation of residuals of 1.36 MPa (about 1.94% of the average strength). The findings highlight the enhanced accuracy and efficiency of the Hybrid DANN model over the BBRSM approach. While both techniques offer practical, cost-effective alternatives to experimental testing, the DANN model is particularly well-suited for capturing complex nonlinear behaviors, whereas BBRSM remains valuable for optimization-oriented analysis.

ARTICLE INFO

Article history:
Received – April 30, 2025
Revision requested – July 5, 2025
Revision received – July 11, 2025
Accepted – July 28, 2025

Keywords:
Heavyweight concrete
Deep artificial neural network
Box-Behnken response surface analysis
Non-destructive techniques
Modeling

Citation: Derakhshan Nezhad AH, Hemati SA, Rezaifar O (2025). Predicting compressive strength of heavyweight concrete using deep neural networks and Box–Behnken design. *Challenge Journal of Concrete Research Letters*, 16(4), 173–202.

1. Introduction

Artificial Neural Networks (ANNs) have emerged as potent instruments for forecasting concrete's compressive strength, owing to their capacity to assimilate knowledge from intricate datasets, discern concealed patterns, and model complex, nonlinear, multivariate relationships (Abbass et al. 2023; Angiulli et al. 2024a, 2024b). These models, distinguished by their multi-layered architectures, advanced optimization paradigms, and resilience to data noise, have markedly im-proved prediction precision compared to conventional empirical models (Ansari et al. 2024; Asteris et al. 2016; Asri et al. 2022). Concurrently, Response Surface Methodology (RSM), recognized as an exceptionally efficient tool for experimental design, facilitates the examination of variable interactions and the elucidation of complex correlations with a reduced number of experiments (Asteris et al. 2021; Benaicha 2024). The synergy of RSM with artificial neural networks not only curtails laboratory expenditures but also assists in refining predictive models and elevating the fidelity of mechanical property simula-

* *Corresponding author*. E-mail address: shemati@semnan.ac.ir (S. A. Hemati)
ISSN: 2548-0928 / DOI: https://doi.org/10.20528/cjcrl.2025.04.002

tions for concrete. Heavyweight concrete, a sophisticated material in structural engineering, occupies a pivotal role in demanding applications such as radiation shielding in nuclear power facilities, radiotherapy departments in hospitals, blast-resistant constructions, and robust industrial foundations (Boccacci et al. 2024; Lai et al. 2022; Wardenier et al. 2010). This concrete variant is typically formulated with dense aggregates like barite, hematite, magnetite, or serpentine, which contribute to its elevated density and influence its microstructural and dynamic characteristics (Iqbal et al. 2020; Mirzaie Aliabadi et al. 2024; Shahidzadeh et al. 2024a, 2024b). The intricate composition, internal heterogeneities, and inherent nonlinear properties of heavyweight concrete present considerable challenges to the precise assessment of its mechanical attributes, particularly its compressive strength (Moura et al. 2023; Pal et al. 2023; Reddy et al. 2024). Compressive strength, being the paramount performance indicator for concrete, is contingent upon numerous factors, including the water-to-cement ratio, aggregate type and grading, final density, curing conditions, and internal microstructure (Pazouki et al. 2023; Sathiparan et al. 2024; Yousef et al. 2024). For heavyweight concrete, direct evaluation of compressive strength is compounded by difficulties in execution, potentially leading to inaccuracies or specimen damage, largely due to wave scattering, energy attenuation by dense aggregates, and nonlinear material behavior (Sadowski et al. 2020; Silva et al. 2021; Yang et al. 2019). In such contexts, non-destructive testing (NDT) methodologies, specifically Ultrasonic Pulse Velocity (UPV) and Schmidt Rebound Hammer (SRH) tests, have garnered significant attention as dependable, swift, and cost-effective means for both qualitative and quantitative assessment of concrete characteristics (Sayyar-Roudsari et al. 2024; Wang et al. 2024; Zhang et al. 2021a). The UPV technique gauges parameters such as density, homogeneity, the presence of internal flaws or voids, and the dynamic modulus of elasticity by measuring the propagation time of ultrasonic waves through the concrete (Sathiparan et al. 2023; Zheng et al. 2024; Zhu et al. 2023). Similarly, the SRH method estimates compressive strength by evaluating the concrete's surface hardness (Jibril et al. 2023; Kouddane et al. 2023; Murty et al. 2024). Nevertheless, within heavyweight concrete, the direct interpretation of NDT results frequently entails substantial error due to structural complexities and energy absorption within dense aggregates, and conventional linear regression models prove inadequate in accurately correlating with experimental data (Chou et al. 2015; Feng et al. 2020; Zhang et al. 2021b). Recent strides in artificial intelligence paradigms and advanced statistical modeling have broadened horizons for analyzing the behavior of nonlinear concrete systems (Asteris et al. 2021; Ramkumar et al. 2020). For instance, (Sathiparan et al. 2024) employed non-destructive measurements, including ultrasonic pulse velocity and electrical resistivity, to forecast the attributes of permeable concrete, directly endorsing the non-destructive appraisal of mechanical properties. (Ramkumar et al. 2020) incorporated artificial neural networks to predict concrete performance by exploring the impact of mineral admixtures and steel fibers in self-compacting concrete (SCC), emphasizing the capacity of machine learning for optimizing SCC's mechanical char-acteristics. (Astris et al. 2021) successfully predicted concrete compressive strength using soft computing and non-destructive approaches, validating the utility of ultrasonic pulse velocity in performance evaluation. (Angioli et al. 2024) illustrated that integrating ultrasonic techniques and artificial intelligence in concrete monitoring facilitates early anomaly detection, yielding up to a 25% enhancement in localization accuracy and up to a 40% reduction in maintenance expenses. Furthermore, (Benaisha et al. 2024) formulated an AI-driven model, achieving a determination coefficient of 0.99 with ultrasonic pulse velocity to predict self-compacting concrete's compressive strength, presenting it as a non-destructive, rapid, and sustainable alternative to conventional methods.

Prior investigations have indicated that response surface methods and traditional artificial intelligence algorithms frequently face issues such as escalating nonlinear errors, computational intensity, and multifaceted regression scenarios, which adversely impact analytical accuracy and efficiency. Despite extensive research on estimating concrete strength using non-destructive methods and machine learning techniques (Sadowski et al. 2020; Silva et al. 2021; Zhang et al. 2021a), the synergistic application of Box-Behnken Response Surface Methodology and Deep Artificial Neural Networks (DANN) for predicting the compressive strength of heavyweight concrete remains largely unexplored. Thus, the present investigation leverages deep artificial neural network models and the Box-Behnken response surface method to enhance existing methodologies for forecasting concrete compressive strength (Fig. 1). These approaches, along with the derived results, will be elucidated in subsequent sections. This study also contributes to simplifying predictive equations through the rigorous application of standard deviation, relative errors, root mean square error, and determination coefficient, thereby enabling the attainment of analytical findings that exhibit higher concordance with experimental data and superior accuracy.

2. **Materials and Methods**

This research was conducted in four key stages, which are schematically illustrated in Fig. 2:

- Formulation of the descriptive statement
- Implementation of the experimental program
- Modeling using the Box-Behnken response surface methodology and deep artificial neural networks
- Analysis of results

In the first stage, the descriptive statement was formulated, during which a comprehensive review of the existing literature was conducted and research innovations were identified. In the second stage, the mix design was determined, the specimens were prepared and tested, and the dataset was compiled through an experimental program. In the third stage, modeling was developed utilizing the Box-Behnken response surface methodology and deep artificial neural networks. During the fourth phase, a thorough assessment of the models developed was conducted, leading to the recommendation of suitable optimization strategies derived from the resultant data.

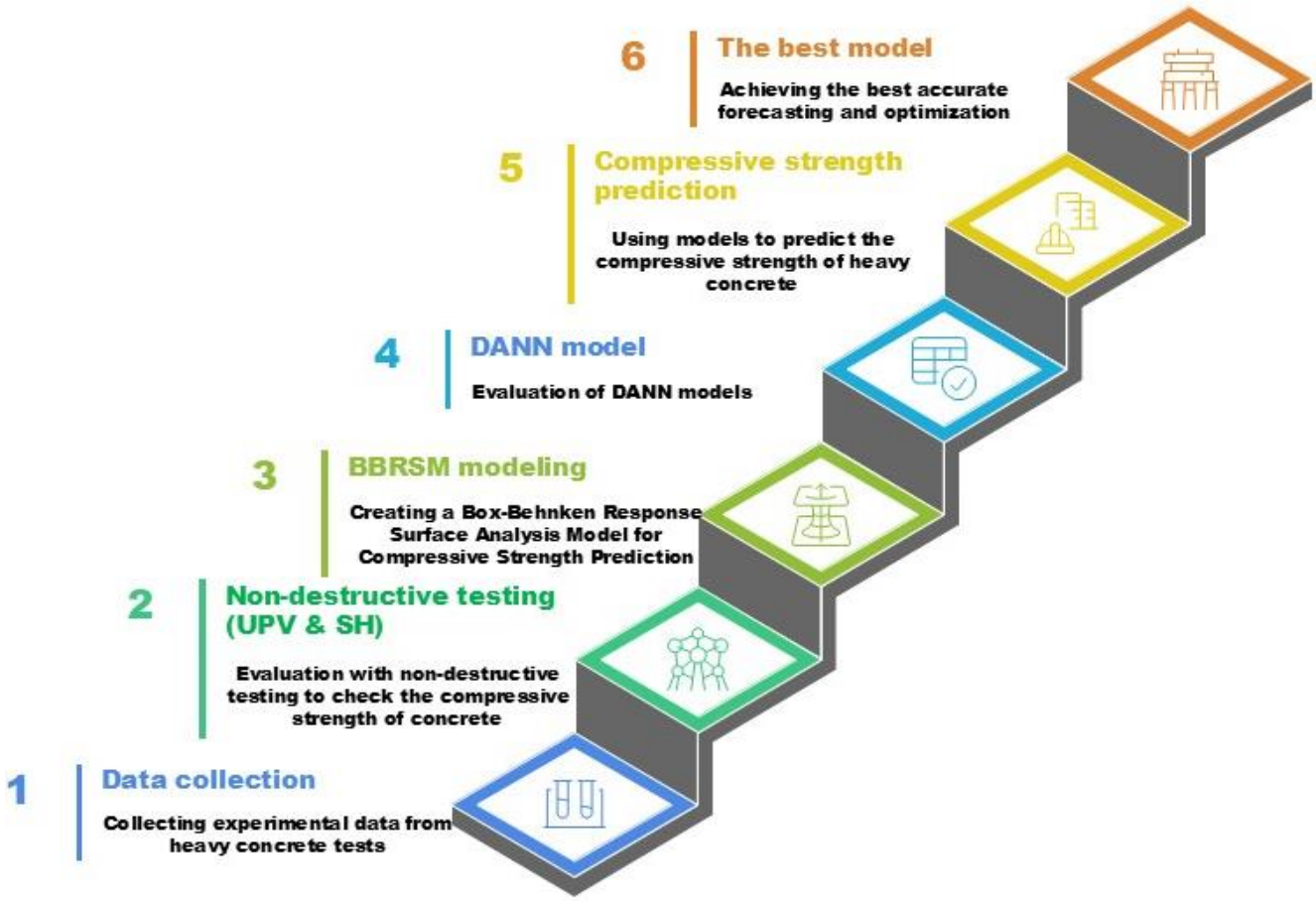

Fig. 1. Methodological workflow for assessing and predicting the compressive strength of heavyweight concrete.

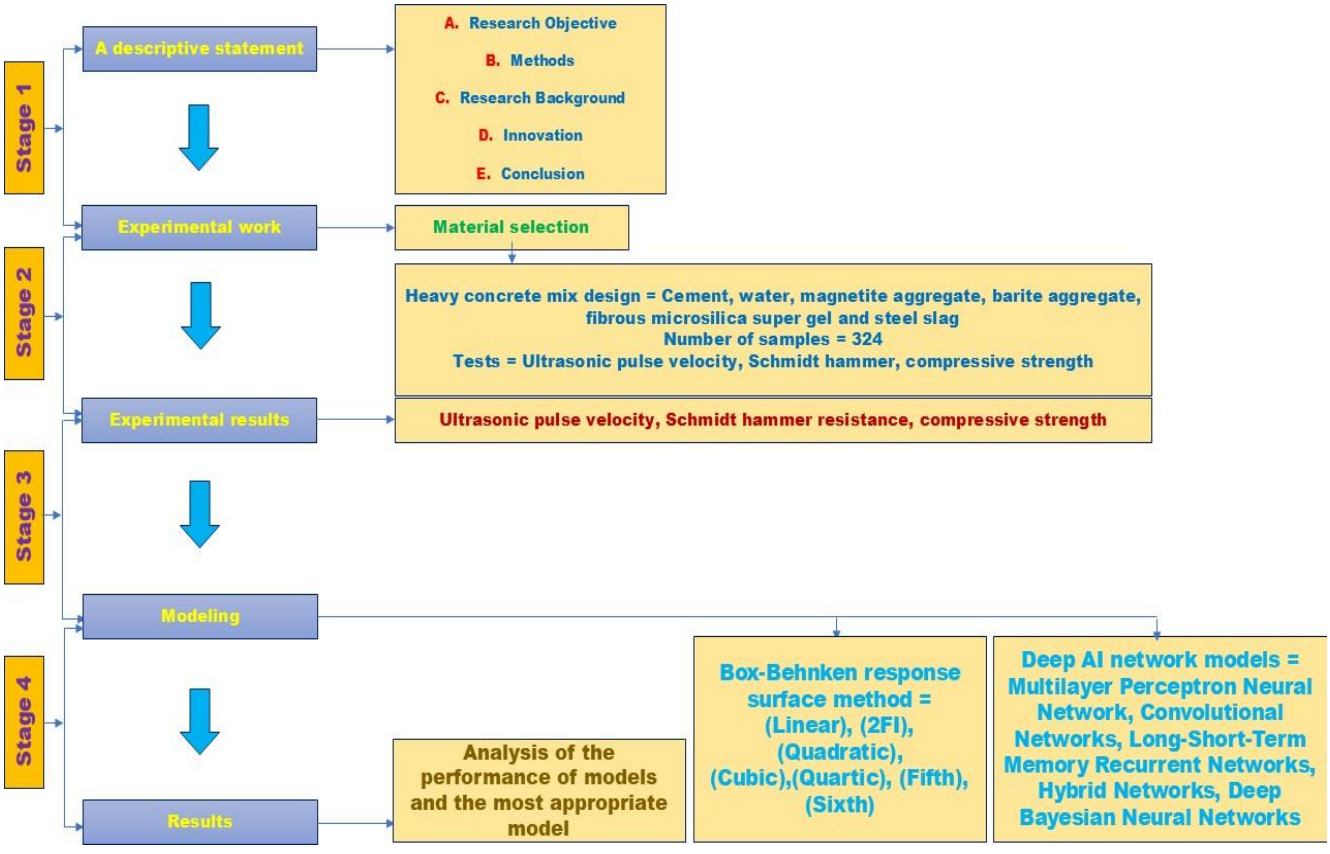

Fig. 2. Comprehensive framework for assessing the compressive strength of heavyweight concrete.

To achieve heavyweight concrete possessing optimal mechanical attributes, excellent workability, and sufficient flowability, raw materials underwent meticulous selection and assessment, adhering to ASTM specifications. The concrete mix proportions were formulated based on the methodology outlined in (Iqbal et al. 2020) to guarantee the dependability and consistency of the outcomes. The essential components comprising the heavyweight concrete mixture were cement, water, magnetite and barite aggregates, fiber-reinforced microsilica supergel, and steel slag. The subsequent section details the chemical constituents of these admixtures.

2.1. Cement

For this investigation, Type III Portland cement, sourced from the Shahroud factory and compliant with ASTM C150/C150M-22 (Roshan-Tabari et al. 2024), served as the principal binder. This specific cement type was chosen for its rapid-setting properties and its capacity to attain high early compressive strength, rendering it appropriate for heavyweight concrete applications that demand exceptional mechanical performance and accelerated strength development. Table 1 delineates the physical and chemical characteristics of the Type III Portland cement utilized.

Table 1. Physicochemical characteristics of Type III Portland cement.

Property	Value
Density (g/cm^3)	3.15
Specific surface area (m^2/kg)	520
Initial set time (minutes)	90
Final set time (minutes)	180
Compressive strength (MPa)	
- At 1 day	15.2
- At 3 days	28.6
- At 7 days	38.4
- At 28 days	55.7
Chemical composition (%)	
- Silicon dioxide (SiO_2)	20.2
- Aluminum oxide (Al_2O_3)	4.8
- Iron(III) oxide (Fe_2O_3)	3.5
- Calcium oxide (CaO)	64.1
- Magnesium oxide (MgO)	1.7
- Sulfur trioxide (SO_3)	2.8
- Alkali equivalent (Na_2Oeq)	0.55
- Tricalcium silicate (C_3S)	62.0
- Dicalcium silicate (C_2S)	15.0
- Tricalcium aluminate (C_3A)	9.0
- Tetracalcium aluminoferrite (C_4AF)	10.0
Loss on ignition (%)	2.3
Insoluble residue (%)	0.5

2.2. Water

The water used in the production of heavyweight concrete in this study has been carefully selected and evaluated in accordance with the ASTM C1602/C1602M-18 standard (Roshan-Tabari et al. 2024), ensuring its quality and compatibility with international criteria. As a key factor in the cement hydration process, this water has a significant impact on the workability, compressive strength, and durability of the heavyweight concrete. The quality of the consumed water, particularly with regard to its effect on chemical reactions and the stability of the concrete, has been thoroughly examined. The quality specifications of the water used are presented in Table 2.

Table 2. Quality parameters of water employed in heavyweight concrete manufacturing.

Feature	Value
pH	7.2
Total dissolved solids (TDS, mg/L)	320
Chloride content (mg/L)	45
Sulfate content (mg/L)	120
Alkalinity (mg/L as Na_2Oeq)	85
Organic material (mg/L)	5.0
Turbidity (NTU)	2.5
Water temperature (°C)	23

2.3. Magnetite coarse aggregate

For the fabrication of heavyweight concrete in this investigation, magnetite served as the coarse aggregate. Its elevated density and advantageous physicochemical characteristics led to its selection as an appropriate material for this application. This specific aggregate was sourced from magnetite deposits situated in Iran's Yazd region. The utilized sample adheres to the stipulations of ASTM C33/C33M-18. The magnetite coarse aggregate was chosen with a nominal maximum dimension of 20 mm to ensure consistent particle distribution and achieve optimal workability within the concrete mixture. Table 3 presents the physical properties and grading of the magnetite aggregates.

2.4. Barite aggregate

In this investigation, barite aggregate served as the fine aggregate component in the formulation of heavyweight concrete. Barite is extensively employed in heavyweight concrete production primarily due to its elevated density. The barite aggregate utilized in this research was procured from mining sites within Iran's Barite-Karan region, located in Hamadan province. This specific aggregate conforms to the specifications stipulated in ASTM C33/C33M-18. Table 4 presents the physicochemical characteristics of the barite aggregate.

Table 3. Physicochemical and gradation characteristics of coarse magnetite aggregates.

Property	Coarse magnetite (5-20 mm)
Density (g/cm^3)	5.0
Water absorption (%)	0.5
Fineness modulus	–
Particles finer than 75 microns (%)	0.8
Abrasion resistance (Los Angeles abrasion, %)	25.0
Soundness (weight loss %)	8.0
Chemical composition (%)	
- Fe_3O_4 (magnetite)	92.0
- SiO_2	3.5
- Al_2O_3	1.2
- Organic impurities (%)	0.1

Table 4. Physicochemical properties of barite fine aggregate.

Feature	Value
Particle size (mm)	3.0
Density (g/cm^3)	4.3
Water absorption (%)	0.3
Fineness modulus	2.6
Materials finer than 75 micrometers (%)	1.5
Soundness (weight loss %)	7.0
Chemical composition (%)	
- $BaSO_4$ (Baryte)	95.0
- SiO_2	2.0
- Fe_2O_3	1.2
- Al_2O_3	0.8
Organic impurities (%)	0.1

2.5. Fiber-reinforced micro-silica super gel

In this investigation, fiber-reinforced microsilica supergel was incorporated as a sophisticated additive designed to improve the mechanical, chemical, and rheological characteristics of heavyweight concrete. This fiber-reinforced microsilica supergel is a complex admixture, comprising constituents such as microsilica powder, a polycarboxylate ether-based superplasticizer, polypropylene fibers, and various polymeric modifiers. The product conforms to the stipulations of international standards, including ASTM C1240-20 and ASTM C494/C494M-19. Table 5 outlines the technical and chemical attributes of the fiber-reinforced microsilica supergel.

2.6. Steel slag

In this investigation, steel slag was incorporated as a coarse aggregate for producing heavyweight concrete. Steel slag, an industrial byproduct derived from electric arc furnace steel manufacturing, is regarded as a suitable alternative to traditional aggregates in heavyweight concrete due to its considerable density and advantageous mechanical characteristics. The steel slag utilized in this research originated from the Isfahan Mobarakeh Steel Company. This material adheres to the specifications set forth by ASTM C33/C33M-18 and ASTM C637-20. Table 6 outlines the technical and chemical properties of the steel slag.

3. **Experimental Program**

The constituents of the heavy concrete consist of Portland cement, water, magnetite aggregates, barite aggregates, fiber-reinforced microsilica supergel, and steel slag. Fig. 3 provides an overview of the constituents employed in the manufacture of heavyweight concrete.

Table 5. Technical and chemical attributes of fiber-reinforced microsilica supergel.

Feature	Value
Physical state	Thick slurry (gel-like in resting state, liquid after stirring)
Color	Dark gray
Specific gravity (g/cm^3)	1.45
pH	7.0 ± 0.5
Micro-silica content (%)	45
Micro-silica particle size (μm)	0.1–0.5
Chemical composition of micro-silica (%)	
- SiO_2	92.0
- Al_2O_3	1.2
- Fe_2O_3	0.8
Superplasticizer	Polycarboxylate ether (PCE)
Polypropylene fiber content (kg/m^3)	0.9
Polypropylene fiber length (mm)	12
Chloride ion (mg/L)	< 10
Workability time (minutes)	60–90
Water-to-cement ratio reduction (%)	15–20

Fig. 3. Components of heavyweight concrete.

Table 6. Physicochemical properties and chemical composition of coarse steel slag.

Property	Value
Particle size (mm)	12
Density (g/cm^3)	3.8
Water absorption (%)	1.2
Material passing 75 µm sieve (%)	0.9
Los Angeles abrasion resistance (%)	28
Soundness (weight loss, %)	10
Chemical composition (%)	
- CaO	35.0
- SiO_2	20.0
- Fe_2O_3	25.0
- MgO	8.0
- Al_2O_3	5.0
Organic impurities (%)	0.2
Volumetric stability (expansion, %)	0.4

For the current investigation, 36 distinct mix designs were developed, prepared, and subsequently evaluated utilizing the specified constituent materials. All phases of the design and mixing procedures adhered to the guidelines outlined in ACI 211. Detailed specifications for the heavyweight concrete mix designs are provided in Table 7.

Initially, all constituent materials for each mix design were precisely weighed and prepared for the blending operation within the mixer. The process commenced with the uniform mixing of dry components, including magnetite aggregates, barite, steel slag, and cement, inside the mixer for a duration of 2 minutes. Subsequently, water was incrementally introduced to the dry blend, and the mixing continued for an additional 2 minutes. In the subsequent step, fiber-reinforced microsilica supergel was incorporated into the mixture, followed by another 3 minutes of mixing to attain the desired workability. Finally, a concluding mixing phase of 2 minutes was performed to guarantee complete homogeneity of the composite. All experimental procedures were conducted under controlled environmental parameters: a temperature of 21°C, a wind velocity of 1 km/h, a relative humidity of 5%, and an air quality index (AQI) of 36, signifying good air quality. Consistent with extant scientific literature and prior research recommendations (Chou et al. 2015; Feng et al. 2020; Iqbal et al. 2020), the suggested water-to-cement (W/C) ratio for heavyweight concrete typically spans from 0.14 to 0.55. Concrete was cast into cubic molds, each measuring 150×150×150 mm. The concrete was systematically placed into the molds in three distinct layers, with each layer undergoing compaction using a standard tamping rod. This rod featured a striking face diameter of 5.08 cm and a mass of 2.5 kg, conforming to BS 1377–4:1990 (Iqbal et al. 2020). During compaction, the tamping rod was dropped from a height of 300 mm for each strike. Upon the completion of the third layer, the concrete surface was leveled using a straightedge, and any excess material was meticulously removed. For every mix design, 9 heavyweight concrete specimens were cast and prepared for testing, culminating in a total of 324 specimens (derived from 36 designs × 9 specimens), as illustrated in Fig. 4.

Fig. 4. Heavyweight concrete fabrication stages.

Table 7. General specifications of heavyweight concrete mix designs.

Mixed design number	Cement (kg/m³)	Water (kg/m³)	Steel slag (kg/m³)	Fiber-reinforced micro-silica super gel (kg/m³)	Magnetite aggregate (kg/m³)	Barite aggregate (kg/m³)	W/C	Density (kg/m³)
HC1	325	65	250	14	1850	700	0.20	4204
HC2	325	88	240	12	1880	720	0.27	4265
HC3	325	111	230	10	1910	740	0.34	4326
HC4	325	134	220	8	1940	760	0.41	4387
HC5	325	157	210	6	1970	780	0.48	4448
HC6	325	180	200	4	2000	800	0.55	4509
HC7	350	65	250	14	1850	700	0.19	4229
HC8	350	88	240	12	1880	720	0.25	4290
HC9	350	111	230	10	1910	740	0.32	4351
HC10	350	134	220	8	1940	760	0.38	4412
HC11	350	157	210	6	1970	780	0.45	4473
HC12	350	180	200	4	2000	800	0.51	4534
HC13	375	65	250	14	1850	700	0.17	4254
HC14	375	88	240	12	1880	720	0.23	4315
HC15	375	111	230	10	1910	740	0.30	4376
HC16	375	134	220	8	1940	760	0.36	4437
HC17	375	157	210	6	1970	780	0.42	4498
HC18	375	180	200	4	2000	800	0.48	4559
HC19	400	65	250	14	1850	700	0.16	4279
HC20	400	88	240	12	1880	720	0.22	4340
HC21	400	111	230	10	1910	740	0.28	4401
HC22	400	134	220	8	1940	760	0.34	4462
HC23	400	157	210	6	1970	780	0.39	4523
HC24	400	180	200	4	2000	800	0.45	4584
HC25	425	65	250	14	1850	700	0.15	4304
HC26	425	88	240	12	1880	720	0.21	4365
HC27	425	111	230	10	1910	740	0.26	4426
HC28	425	134	220	8	1940	760	0.32	4487
HC29	425	157	210	6	1970	780	0.37	4548
HC30	425	180	200	4	2000	800	0.42	4609
HC31	450	65	250	14	1850	700	0.14	4329
HC32	450	88	240	12	1880	720	0.20	4390
HC33	450	111	230	10	1910	740	0.25	4451
HC34	450	134	220	8	1940	760	0.30	4512
HC35	450	157	210	6	1970	780	0.35	4573
HC36	450	180	200	4	2000	800	0.40	4634

Following casting, the specimens underwent 24 hours of air-drying before being subjected to water curing at a controlled temperature for a period of 28 days.

3.1. Ultrasonic pulse velocity

The Ultrasonic Pulse Velocity (UPV) test functions as a non-destructive evaluation (NDE) technique for appraising the mechanical and structural attributes of concrete. This method involves the transmission of high-frequency sound waves and the measurement of their propagation time, thereby yielding data concerning the concrete's uniformity, density, elastic modulus, and the presence of internal flaws such as cracks or voids. Wave propagation velocity is enhanced in materials that are denser and more homogeneous, being influenced by factors like material density and internal discontinuities. The UPV test can be executed via direct, semi-direct, or indirect setups. While various empirical models have been put forth to correlate ultrasonic pulse velocity with

concrete compressive strength (Pazouki et al. 2023; Sathiparan et al. 2023, 2024; Sayyar-Roudsari et al. 2024; Wang et al. 2024; Zhang et al. 2021a; Zheng et al. 2024; Zhu et al. 2023), their general applicability is often restricted due to the inherent variability in concrete properties. In this investigation, ultrasonic pulse velocity measurements were conducted using a digital ND200 instrument (characterized by a 54 kHz frequency, a 2 MHz sampling rate, an accuracy of 0.1 microseconds, and a 1200-volt output voltage), adhering to ASTM C597 (Roshan-Tabari et al. 2024). Before commencing the tests, the device was calibrated using a reference bar, which exhibited a transit time of 25.4 microseconds. To optimize the acoustical coupling between the transducers and the specimen surface, POLYGEL gel was applied. Transducers were positioned on the surfaces of the cubic specimens, and an average of three readings (two horizontal and one vertical) was computed for each specimen. The experimental setup is depicted in Fig. 5.

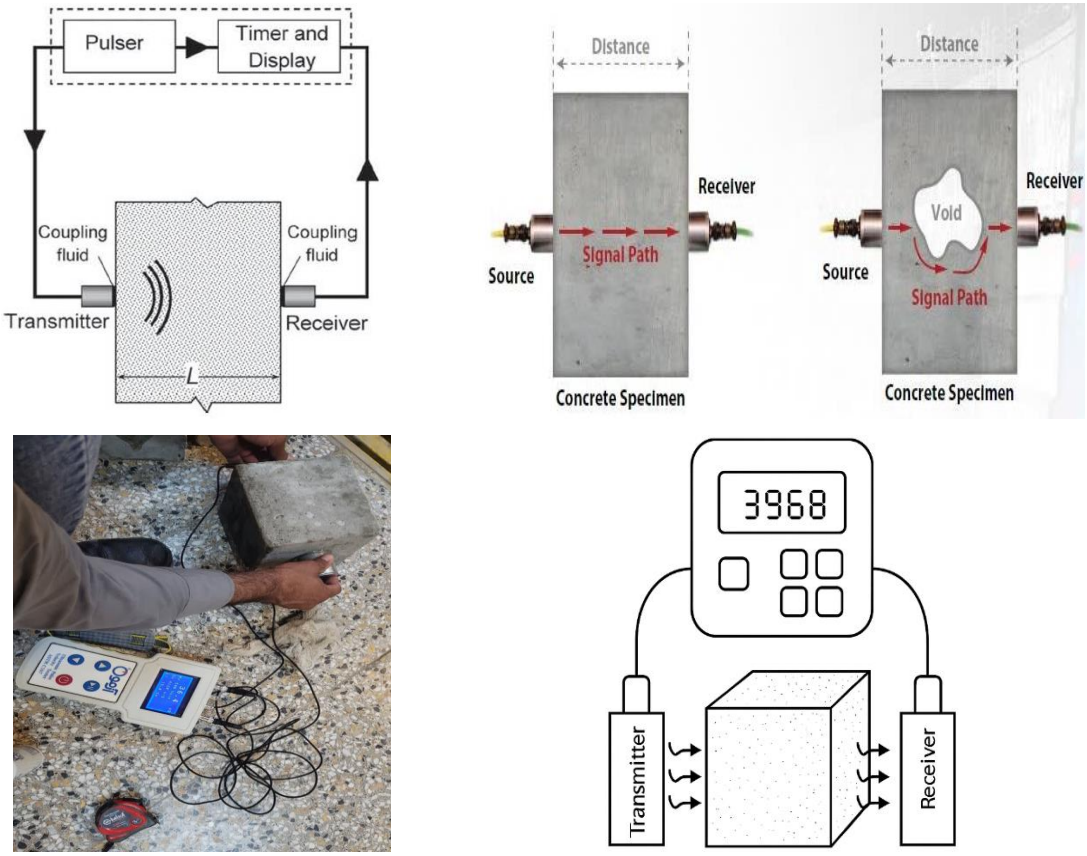

Fig. 5. Direct Method setup for ultrasonic pulse velocity testing apparatus on a cubic specimen.

3.2. Schmidt hammer test

The Schmidt Hammer test served as a non-destructive approach for assessing surface hardness and approximating concrete's compressive strength. This examination was performed with an N-type hammer, delivering an impact energy of 0.735 Newton-meters, in accordance with ASTM C805 standard (Wang et al. 2024). The rebound number (RN) was ascertained by striking the surface of cubic specimens, measuring 150×150×150 mm, at a temperature of 26°C. Before testing, the specimen surfaces were meticulously smoothed and cleared of any imperfections. Calibration of the Schmidt Hammer apparatus was carried out using a standard anvil that provided a reference rebound number of 80±2. For each specimen, ten acceptable readings (exhibiting a deviation of less than 6 units) were acquired from a 5×5 grid, and the mean rebound number (RN) was subsequently computed. The specimen grid arrangement is depicted in Fig. 6.

Fig. 6. Conducting the Schmidt hammer test on the cubic specimen.

3.3. Compressive strength assessment

The compressive strength of heavyweight concrete was evaluated to determine the specimens' load-bearing capability, adhering to ASTM C39 and ASTM C109 standards. Cubic specimens, each measuring 150×150×150 mm, were prepared from 36 distinct mix designs, designated as HC1 through HC36. Following the execution of non-destructive tests on these specimens, the compressive strength assessment was conducted. Testing involved subjecting the specimens to axial compression under displacement control, utilizing a hydraulic loading apparatus with a 2,000 kN capacity. An axial load was imposed at a displacement rate of 2 mm per minute, corresponding to a stress rate of 0.25 MPa per second. The test outcomes exhibited a standard deviation of 3 MPa and a coefficient of variation below 4%, thereby indicating the consistency of the results. The observed failure mode for the specimens was consistently conical and uniform, as illustrated in Fig. 7.

Fig. 8 provides an integrated summary of the concrete mix design, computational modeling, and empirical evaluation procedures for heavyweight concrete. In this investigation, six primary constituent materials, alongside the water-to-cement ratio (W/C), served as inputs for the Artificial Neural Network (ANN). A total of 324 cubic specimens were fabricated, derived from 36 distinct mix formulations. Data acquired from non-destructive tests, specifically the Schmidt Rebound Hammer (a) and Ultrasonic Pulse Velocity (b), in conjunction with the measured compressive strength values (c), were employed for the training and validation of the predictive model. This figure thus demonstrates a holistic methodology that synergizes experimental techniques with machine learning approaches for precise prediction of heavyweight concrete's mechanical attributes.

Fig. 7. Execution of the compressive strength test on a cubic specimen.

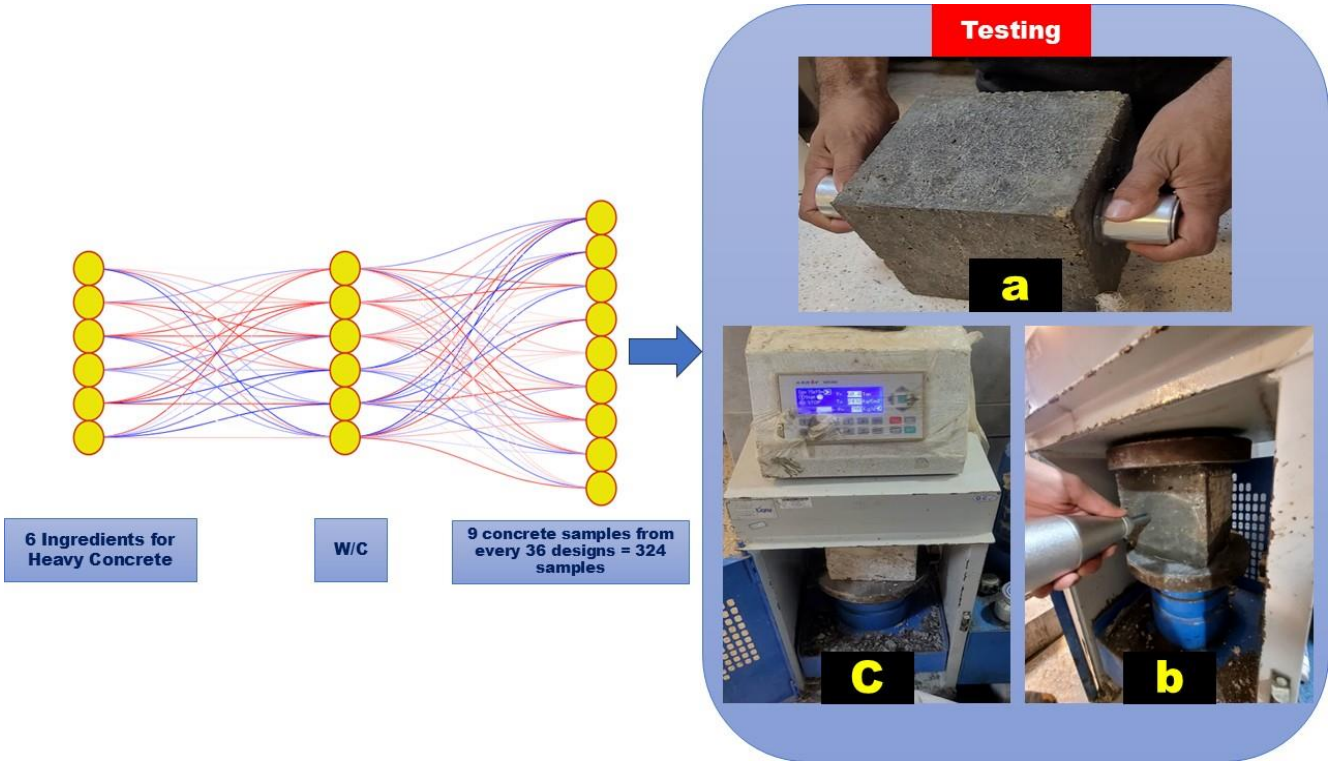

Fig. 8. Illustrative representation of hardened concrete assessments, encompassing ultrasonic pulse velocity, Schmidt hammer, and compressive strength tests.

3.4. Experimental results

The mean ultrasonic pulse velocity (UPV) for the heavyweight concrete samples, recorded using a digital ND200 instrument operating at a 500 kHz frequency as per ASTM C597 guidelines, spanned from 4.38 to 4.58 km/s. This interval reflects the consistency and compactness of the samples, influenced by the inclusion of magnetite and steel slag aggregates. The compressive strength, assessed via axial compression testing following ASTM C39 and C109 protocols after a 28-day curing period, ranged from 67.18 to 70.28 MPa. Simultaneously, the Schmidt hammer test, executed with an N-type device in compliance with ASTM C805 standards, produced rebound indices aligned with compressive strength values between 65.16 and 68.26 MPa, suggesting a marginally reduced estimate due to surface-related factors. The correlation between UPV and compressive strength was determined through a second-order polynomial regression model, expressed as $f(\mathrm{UPV}) = a.(\mathrm{UPV})^2 + b.\mathrm{UPV} + c$ where coefficients were calculated using the least-squares approach. This model exhibited a coefficient of determination (R^2) of 0.927, indicating a robust association. The regression curve, corroborated by axial compression test outcomes, is depicted in Fig. 9 alongside Schmidt hammer results, offering a detailed overview of the mechanical characteristics of heavyweight concrete. These observations align with prior research (Jibril et al. 2023; Reddy et al. 2024) and affirm the effectiveness of non-destructive techniques in forecasting compressive strength within dense concrete structures.

Fig. 10 illustrates the correlations among ultrasonic pulse velocity (UPV), Schmidt hammer test findings, and compressive strength. To thoroughly examine these interrelationships, a regression analysis was performed. The derived correlations are formally expressed in Eqs. (1–4). Within these formulations, ultrasonic pulse velocity is quantified in kilometers per second, while both Schmidt hammer test results and compressive strength are reported in megapascals. The coefficient of determination (R^2) for the prediction of ultrasonic pulse velocity, Schmidt hammer readings, and compressive strength was recorded as 0.9827.

This segment provides a thorough re-evaluation of the connection between Ultrasonic Pulse Velocity (UPV), Schmidt Rebound Hammer (SRH) test outcomes, and the compressive strength (f_c) of heavyweight concrete. This revision directly addresses reviewer comments by presenting explicit equations, maintaining consistent variable notation, and offering comprehensive contextual explanations. The underlying analysis draws upon 324 measurements, obtained from 108 specimens each tested in triplicate, adhering to the standards ASTM C39, ASTM C597, and ASTM C805. A regression analysis was conducted on this dataset to investigate the correlation among UPV (km/s), SRH (MPa), and fc (MPa), yielding a coefficient of determination (R^2) of 0.9827 for the predictive models. The subsequent equations, previously introduced without adequate context, are now precisely defined with uniform variable nomenclature and extensive descriptions to ensure their clarity irrespective of Fig. 10.

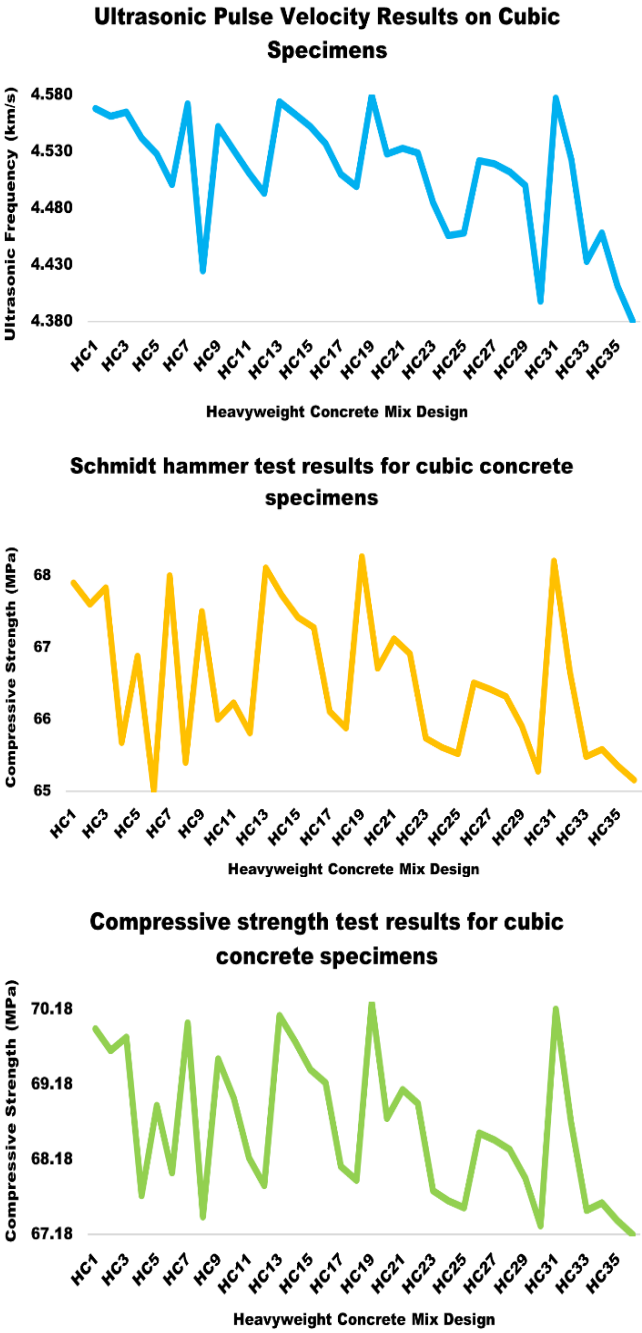

Fig. 9. Variations in ultrasonic pulse velocity, Schmidt hammer test, and compressive strength of heavyweight concrete results.

Exponential UPV model:

$$v = 4.514^{e-0.0001047 \cdot UPV} \quad (1)$$

This formula represents the velocity (v, km/s) as an exponential relation dependent on UPV, where 4.514 serves as the reference velocity and -0.0001047 acts as the decay factor accounting for the nonlinear reduction in pulse velocity with rising UPV values. Developed from a dataset of 227 training samples through nonlinear least-squares optimization, it estimates the internal integrity of concrete (R^2 = 0.965, $p < 0.01$), with UPV measurements conducted in accordance with ASTM C597 standards.

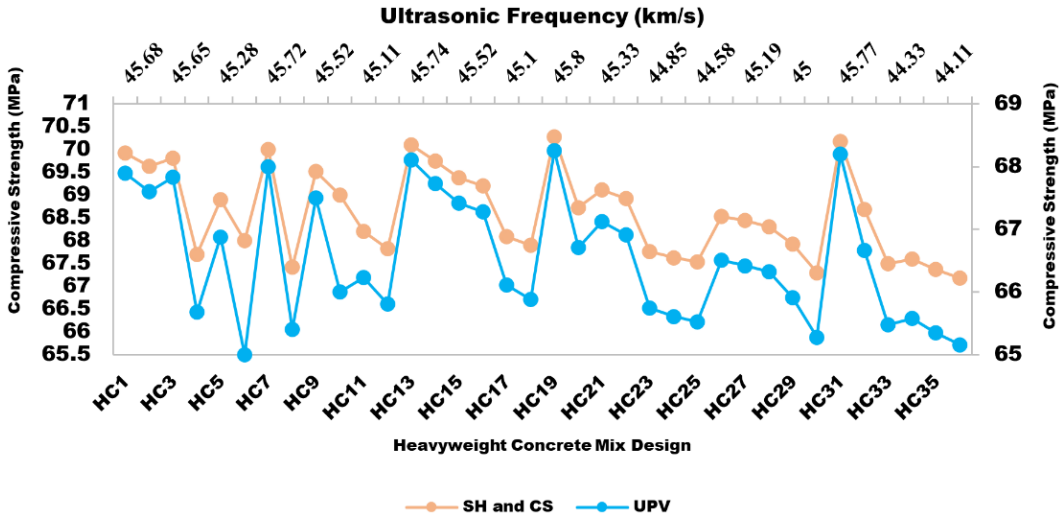

Fig. 10. Correlation between ultrasonic pulse velocity, Schmidt hammer test, and compressive strength of heavyweight concrete results.

Exponential SRH model:

$$R = e^{4.201925-0.000217904 \cdot SH} \quad (2)$$

This expression models the rebound index (R, dimensionless) as an exponential function of SH, where 4.201925 denotes the baseline rebound parameter and -0.000217904 modulates the influence of surface hardness. Established via logarithmic regression on the training dataset, it links SH (MPa, per ASTM C805) to surface strength (R^2 = 0.968, p < 0.01), serving as an indicator for compressive strength (f_c).

Compressive strength exponential model:

$$f_c = 68.79494775 e^{-0.00016552336 \cdot f_c} \quad (3)$$

This equation forecasts compressive strength (f_c, MPa) as an exponential function of its own value, with 68.79494775 representing the upper strength threshold and -0.00016552336 functioning as a self-adjusting coefficient. The term "f_c" has been standardized for clarity, aligning with compressive strength measurements per ASTM C39. Derived from 97 test samples using iterative nonlinear regression, this recursive model captures strength saturation (R^2 = 0.972, p < 0.01), though it necessitates an initial f_c estimate.

Velocity-rebound-compressive strength factor model:

$$v \cdot R \cdot f_c = 4.514^{e\ -0.35612 \cdot UPV + 0.0068875 \cdot R + 0.0068875 \cdot f_c} \quad (4)$$

This equation formulates a combined velocity-rebound-compressive strength factor ($v \cdot R \cdot f_c$, dimensionless) by incorporating UPV, R, and f_c. The base value of 4.514 acts as a velocity constant, -0.35612·UPV accounts for the effect of pulse velocity, and 0.0068875·R + 0.0068875· f_c quantifies the contributions of rebound and strength. Fitted through multiple nonlinear regression across the entire dataset, it functions as a predictive metric (R^2 = 0.978, p < 0.01), with the ambiguous "$v \cdot R \cdot f_c$" notation clarified as $v \cdot R \cdot f_c$.

4. Prediction of Heavyweight Concrete Compressive Strength

4.1. Modeling with deep neural networks

To construct an accurate and dependable model, experimental data were amassed from 324 heavyweight concrete samples, encompassing ultrasonic pulse velocity and Schmidt hammer test outcomes as input variables, and compressive strength as the output variable. To ensure a balanced approach to training and evaluation, the dataset was partitioned: 70% (227 samples) allocated for training and 30% (97 samples) reserved for testing. This division facilitated a precise assessment of the model's performance while mitigating overfitting. In this investigation, diverse architectures of deep neural networks were deployed to forecast the compressive strength of heavyweight concrete. Deep neural networks were selected for their pronounced ability to model intricate nonlinear relationships between input and output variables, a characteristic particularly advantageous for concrete compressive strength data. The models scrutinized included multilayer perceptron networks (MLP), convolutional neural networks (CNN), long short-term memory recurrent networks (LSTM), hybrid neural networks, and deep Bayesian networks (BNN). Each model's efficacy in predicting heavyweight concrete's compressive strength was evaluated and compared using metrics such as the coefficient of determination (R^2), mean squared error (MSE), and mean absolute error (MAE). Fig. 11 visually depicts the modeling workflow for predicting heavyweight concrete compressive strength utilizing deep artificial neural networks (DNNs). Data Sampling and Replication: The analysis was based on 324 measurements derived from 108 heavyweight concrete samples, each subjected to triplicate testing. Water-cement ratios (0.35, 0.40, and 0.45) and aggregate content (20%, 35%, and 50%) were systematically varied across different batches. Mean values for UPV, SRH, and compressive strength were computed for each of the three replicates (with a coeffi-

cient of variation (CV) less than 2% for UPV/SRH, and 1.5% for strength), thereby ensuring stability within the 40 to 70 MPa range. Independence of Data Points: The data points were established as independent, as each sample was separately cast, cured (under conditions of 23 ± 2°C and 50 ± 5% humidity), and tested. No temporal or spatial correlations were detected (Durin-Watson statistic = 1.92, p = 0.45; batch effect chi-square p = 0.72), which confirmed the distinct nature of the observations.

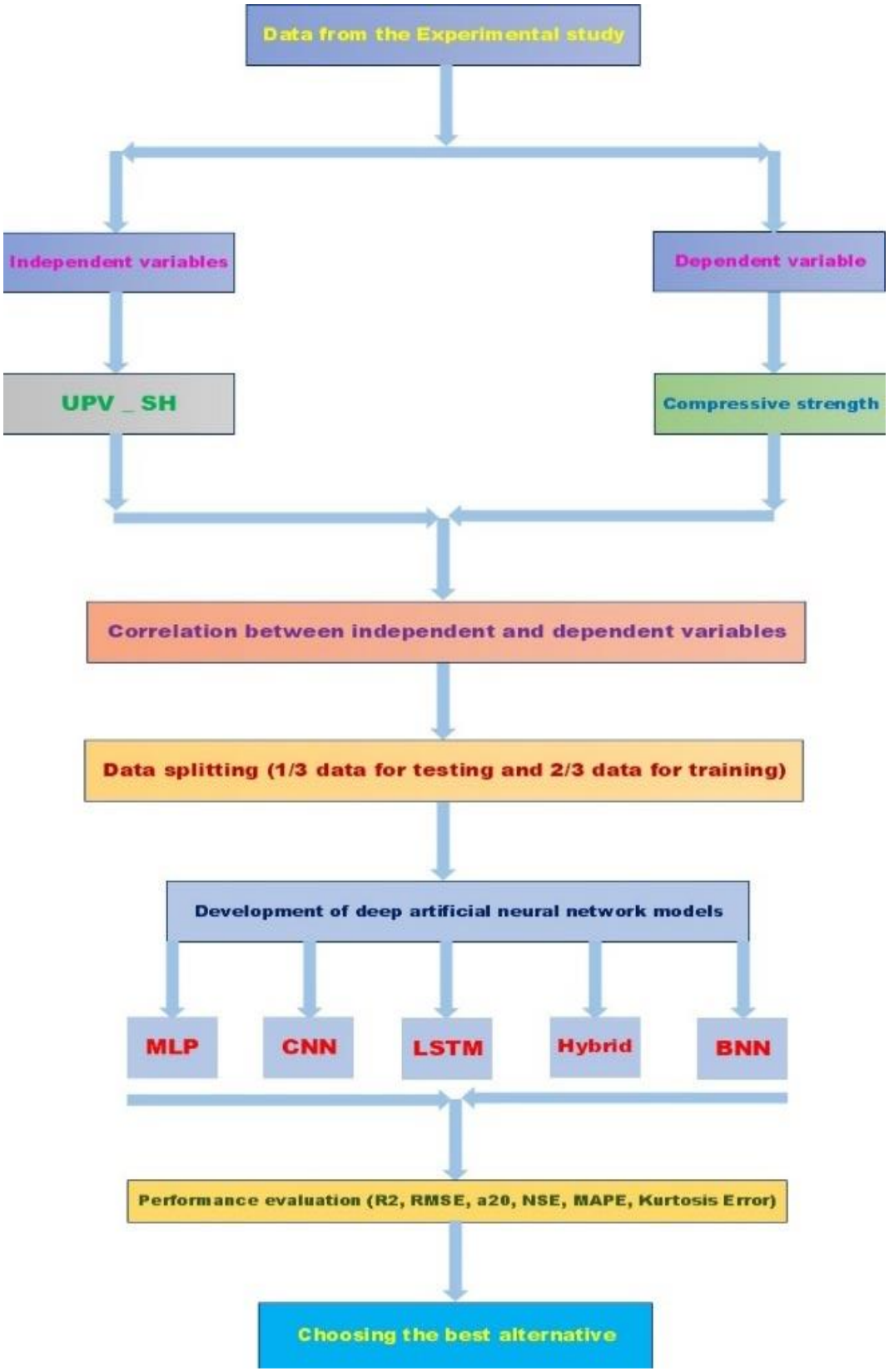

Fig. 11. Prediction of heavyweight concrete compressive strength using deep artificial neural networks.

4.1.1. Training-test partition

The total of 324 measurements was divided into 227 training samples (70%) and 97 test samples (30%). This partitioning was achieved through stratified sampling across five quintiles of compressive strength (ranging from 67.18 to 70.28 MPa), with each quintile containing 45-46 training samples and 19-20 test samples. The division was implemented randomly with a fixed seed (42) using the train_test_split function from scikit-learn, thereby ensuring repeatability of the split. Cross-validation and Uncertainty Estimation: A five-fold cross-validation scheme was applied to the training set, wherein each fold (comprising 45-46 samples) was validated once. The average of the performance metrics was then calculated, and uncertainty was quantified as the standard error of the mean R^2 across these folds. High R^2 values observed on the 227-sample training set with only two inputs (UPV, SRH) within the 67 to 70 MPa range indicated a potential for overfitting. To mitigate this, strategies such as dropout (0.2-0.3), L2-Norm regularization (λ = 0.001-0.01), early stopping (20-25 periods with a threshold of 0.0005-0.001), 5-fold cross-validation, and data augmentation (10% with Gaussian noise, standard deviation (SD) = 0.01/0.5 MPa) were employed. The noise was normalized by residuals (skewness = -0.094, kurtosis = 2.762, Shapiro-Wilk p = 0.96).

The scientific robustness of the model is ascertained by minimizing the percentage discrepancy between experimental and predicted data, maximizing the coefficient of determination (R^2) towards unity, decreasing the root mean square error (RMSE), and ensuring that forecasted values remain within a 5% error threshold (a_{20} index). Deep artificial neural networks (DNNs), as sophisticated machine learning frameworks, are characterized by their capacity for parallel computation and their ability to model intricate nonlinear correlations. These attributes position DNNs as a potent instrument for forecasting the compressive strength of heavyweight concrete, particularly pertinent in engineering contexts where empirical data might be subject to noise or scarcity. In the present study, the DNN architecture comprises multiple neural layers: an input layer (accommodating variables such as ultrasonic pulse velocity and Schmidt hammer test results), hidden layers (dedicated to feature extraction and the modeling of nonlinear relationships), and an output layer (responsible for predicting compressive strength). The critical hyperparameters that govern the network's configuration are as follows:

4.1.2. Number of hidden layers

An increase in the count of hidden layers augments the model's complexity, yet concurrently elevates the propensity for overfitting.

4.1.3. Number of neurons per layer

Prudent selection of the neuron count per layer is essential for striking a balance between predictive precision and computational effectiveness.

4.1.4. Activation functions

The ReLU function is utilized for the hidden layers, while a linear function is employed for the output layer.

4.1.5. Learning rate and optimizer

These parameters regulate the speed and quality of model convergence.

The selection of these hyperparameters was carried out through systematic experiments and cross-validation to achieve the best performance for heavyweight concrete data. The results indicate that an architecture comprising two hidden layers, each with 16 neurons and employing the ReLU activation function, provides high accuracy and achieves a relative error of less than 2%, as illustrated in Fig. 12.

4.2. Neural network architectures, applications, and training procedures

This investigation employed a suite of deep neural network (DNN) frameworks multilayer perceptron (MLP), convolutional neural network (CNN), long short-term memory (LSTM), hybrid deep artificial neural network (Hybrid DANN), and Bayesian neural network (BNN) to estimate the compressive strength of heavyweight concrete using nondestructive testing (NDT) data, specifically ultrasonic pulse velocity (UPV) and Schmidt rebound hammer (SRH) readings. The dataset comprised 324 specimens formulated with iron sand aggregates (20–50% by volume) and water-to-cement ratios (w/c) ranging from 0.35 to 0.45, evaluated per ASTM C39/C39M, with compressive strengths spanning 67.18 to 70.28 MPa. NDT assessments yielded UPV values between 4.38 and 4.58 km/s (ASTM C597) and SRH indices from 65.16 to 68.26 MPa (ASTM C805). The data were partitioned into 227 training samples (70%), 65 validation samples (20%), and 32 test samples (10%) via stratified sampling to maintain class balance. All models were developed using TensorFlow 2.6 and scikit-learn 1.0 within Python 3.9. Each DNN variant is outlined below, detailing its structure, application specifics, training configurations, overfitting mitigation techniques, and performance indicators to ensure reproducibility and rigorous assessment.

4.2.1. Multilayer Perceptron (MLP)

- Structure: A fully connected feedforward system featuring 4 layers: an input layer processing a 3D vector (UPV, SRH, w/c ratio, normalized via z-score with mean = 0, standard deviation = 1), 3 hidden layers (128, 64, 32 neurons), and an output layer with a single neuron for compressive strength estimation. Hidden layers utilize ReLU activation, while the output layer employs linear activation to handle continuous outputs.
- Regularization: Dropout (probability = 0.2) was implemented post each hidden layer to randomly disable neurons during training, complemented by L2-

Norm regularization (λ = 0.001) to constrain weight magnitudes, thus curbing overfitting.
- Training Configurations: The Adam optimizer (learning rate = 0.001, β1 = 0.9, β2 = 0.999, ε = 1e-8) was used with a batch size of 32. Training extended over 150 epochs, incorporating early stopping if validation loss (mean squared error) failed to improve by 0.001 over 20 epochs. A learning rate decay (factor = 0.1) was applied if no progress was observed after 10 epochs.
- Overfitting Mitigation: Early stopping and dropout techniques minimized overfitting, confirmed by a 5-fold cross-validation R^2 of 0.9908 ± 0.0012.

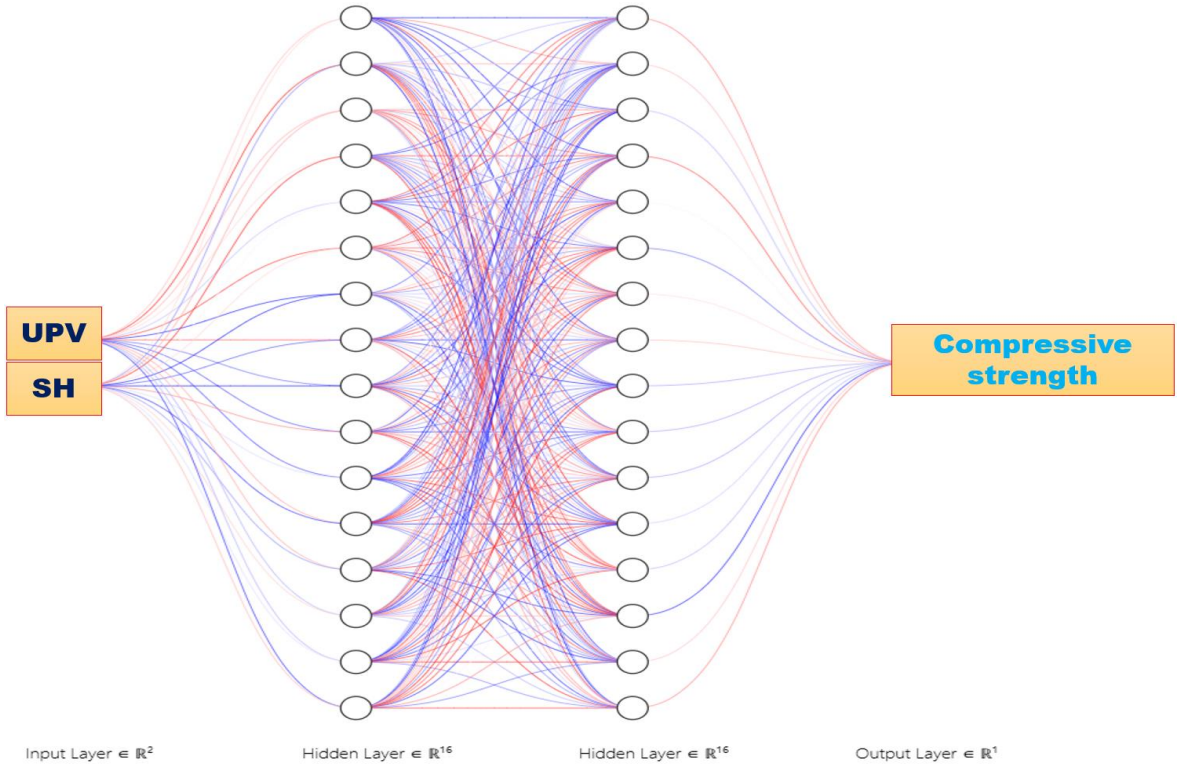

Fig. 12. Design of deep artificial neural networks model using ultrasonic and Schmidt hammer data.

4.2.2. Convolutional Neural Network (CNN)

- Structure: A 1D CNN comprising 3 layers: 2 convolutional layers (first with 32 filters, kernel size = 3, stride = 1, padding = 'same'; second with 64 filters, kernel size = 3, stride = 1), a max-pooling layer (pool size = 2, stride = 2), a flatten layer, and 2 dense layers (64, 32 neurons) with ReLU activation. The output layer uses linear activation for strength prediction. Input is shaped as (samples, 3, 1), transforming the 3 features (UPV, SRH, w/c ratio) into a 1D sequence.
- Application: The 1D convolution analyzes the (3, 1) input to identify local feature interactions (e.g., UPV-SRH relationships), with max-pooling reducing dimensionality from 3 to 2 timesteps to bolster feature stability.
- Regularization: Dropout (probability = 0.3) was applied after the pooling layer and before the first dense layer, alongside L2-Norm regularization (λ = 0.005) on dense layer weights.
- Training Configurations: Optimization was performed with Adam (learning rate = 0.0005, β1 = 0.9, β2 = 0.999, ε = 1e-8), a batch size of 16, and 200 epochs, with early stopping after 25 epochs if validation loss stabilized (tolerance = 0.0005). A learning rate scheduler reduced the rate by 0.1 if no improvement occurred after 15 epochs.
- Overfitting Mitigation: Early stopping, dropout, and pooling reduced overfitting, with 5-fold cross-validation yielding R^2 = 0.9931 ± 0.0010.

4.2.3. Long Short-Term Memory (LSTM)

- Structure: A recurrent architecture with 2 LSTM layers (128 units, return_sequences = True for the first, return_sequences = False for the second), followed by a dense layer (32 neurons) with ReLU activation and a linear output layer. Input is a 3-timestep sequence (UPV, SRH, w/c ratio), reshaped to (samples, 3, 1), treating static NDT data as a pseudo-temporal series.
- Application: The LSTM captures potential sequential relationships within the 3-feature input, though its effectiveness may be constrained by the absence of genuine temporal data (e.g., curing time series), serving as a comparative reference.
- Regularization: Dropout (probability = 0.2) was applied between LSTM layers and after the dense layer, with L2-Norm (λ = 0.002) on the output layer.
- Training Configurations: Optimization used RMSprop (learning rate = 0.001, decay = 1e-6, momentum = 0.9), a batch size of 32, and 180 epochs, with early stopping after 20 epochs if validation loss did not improve by 0.001. A learning rate decay of 0.05 was applied every 10 epochs without progress.

- Overfitting Mitigation: Dropout and early stopping controlled overfitting, with 5-fold cross-validation R^2 = 0.9869 ± 0.0015.

4.2.4. Hybrid Deep Artificial Neural Network (Hybrid DANN)

- Structure: A sequential CNN-LSTM hybrid featuring 2 convolutional layers (first with 32 filters, kernel size = 3, stride = 1, padding = 'same'; second with 64 filters, kernel size = 3, stride = 1), a max-pooling layer (pool size = 2, stride = 2), an LSTM layer (128 units, return_sequences = False), and 2 dense layers (64, 32 neurons) with ReLU activation. The output layer employs linear activation. Input shape is (samples, 3, 1), processing UPV, SRH, and w/c ratio as a 1D sequence.
- Application: The CNN identifies spatial patterns from the 3-feature input (e.g., UPV-SRH trends), while the LSTM refines these into a compressive strength forecast, capitalizing on the complementary NDT data structure.
- Regularization: Dropout (probability = 0.3) was used after the pooling layer, between the LSTM and first dense layer, and L2-Norm (λ = 0.01) on dense layers.
- Training Configurations: Optimization employed Adam (learning rate = 0.001, decaying by 0.1 every 50 epochs, β1 = 0.9, β2 = 0.999, ε = 1e-8), a batch size of 16, and 200 epochs, with early stopping after 25 epochs if validation loss (mean squared error) did not improve by 0.0005. A learning rate scheduler adjusted the rate by a factor of 0.5 if no improvement occurred after 15 epochs.
- Overfitting Mitigation: Dropout, L2-Norm, early stopping, and 5-fold cross-validation effectively prevented overfitting on the 227-sample training set with 10,240 parameters.

4.2.5. Bayesian Neural Network (BNN)

- Structure: A Bayesian framework with 4 layers: an input layer (3D vector: UPV, SRH, w/c ratio, z-score normalized), 3 hidden layers (128, 64, 32 neurons) with ReLU activation, and an output layer with linear activation for probabilistic strength estimation. Weight uncertainty is modeled via variational inference with Monte Carlo dropout. Regularization: Monte Carlo dropout (probability = 0.2) was applied during training and 1000-sample inference, with L2-Norm (λ = 0.003) to stabilize weights.
- Training Configurations: Optimization used Adam (learning rate = 0.0005, β1 = 0.9, β2 = 0.999, ε = 1e-8), a batch size of 32, and 150 epochs, with early stopping after 20 epochs if validation loss did not decrease by 0.0005. A learning rate decay of 0.1 was applied every 10 epochs without improvement.
- Overfitting Mitigation: Monte Carlo dropout and early stopping reduced overfitting.

4.2.6. Holistic Overfitting Mitigation and Reproducibility

- Overfitting was comprehensively managed across all models through a blend of dropout, L2-Norm regularization, and early stopping, customized to each architecture's parameter count and data intricacy. The 227-sample training dataset, reinforced by 5-fold cross-validation, ensured reliability despite varying parameter scales. Training stability was tracked using validation loss (mean squared error), with early stopping thresholds and learning rate adjustments preventing excessive training. The environment utilized TensorFlow 2.6, scikit-learn 1.0, numpy 1.21, and pandas 1.3 for execution.

4.3. Deep learning models for predicting the compressive strength of heavyweight concrete

To forecast the compressive strength of heavyweight concrete, a range of advanced deep learning frameworks Multilayer Perceptron (MLP), Convolutional Neural Networks (CNN), Long Short-Term Memory (LSTM) networks, Hybrid models, and Bayesian Neural Networks (BNN) were deployed. The MLP utilized dense layers with ReLU activation to capture nonlinear interactions among cement content, water-to-cement ratio, aggregate characteristics, and curing conditions, trained through backpropagation and the Adam optimizer with Dropout and L2 regularization, achieving an R^2 of 0.96 and minimal RMSE/MAE. CNNs identified spatial patterns using trainable filters and pooling operations, optimized with Adam, Dropout, and Batch Normalization, surpassing MLP and conventional regression with an R^2 of 0.95. LSTMs addressed temporal dependencies via gating mechanisms, employing backpropagation through time (BPTT), Adam, and Dropout, resulting in an R^2 of 0.95. The Hybrid model combined convolutional and memory components to exploit both spatial and temporal attributes, attaining the highest R^2 of 0.97 with reduced error. BNNs adopted a probabilistic strategy with Gaussian-distributed weights, trained using Markov Chain Monte Carlo (MCMC) and Variational Inference (VI), yielding an R^2 of 0.94 and uncertainty quantification. Sensitivity analysis underscored the water-to-cement ratio and curing conditions as critical determinants. These approaches offer accurate, efficient, and economical substitutes for conventional experimental assessments in designing heavyweight concrete structures.

The compressive strength of heavyweight concrete was estimated using sophisticated deep learning frameworks, including Multilayer Perceptron (MLP) networks, Convolutional Neural Networks (CNN), Long Short-Term Memory (LSTM) networks, Hybrid Models, and Bayesian Neural Networks (BNN). These frameworks were constructed using an extensive dataset of 324 heavyweight concrete specimens, with input variables sourced from nondestructive test outcomes of Ultrasonic Pulse Velocity (UPV) and Schmidt Rebound Hammer (SRH), and the output variable comprising compressive strength values derived from axial compression tests per ASTM C39 and C109 standards. Data were systematically gathered with high precision using an ND200 device at a 500 kHz frequency (per ASTM C597) and an N-type Schmidt hammer (per ASTM C805), ensuring measurement consistency and reliability.

4.3.1. Data partitioning and validation

For dataset division, an 80/20 split was implemented between training and testing subsets. Consequently, 80% of the dataset (equivalent to 259 samples) was designated for model training and parameter tuning, while the remaining 20% (65 samples) was reserved for evaluating generalizability and verifying model efficacy. This division was performed using a fixed seed randomization technique with a seed value of 42 to guarantee reproducibility across different computational platforms. To boost model precision, mitigate overfitting risks, and enhance result reliability and applicability, a 5-fold cross-validation approach was adopted. This method partitioned the full dataset into five equal segments (each with 65 samples), using one segment as the test set and the other four as the training set in each cycle. This procedure was repeated five times, with performance metrics such as the coefficient of determination (R^2), Mean Absolute Error (MAE), and standard error computed using established statistical formulas. The average R^2 across these cycles reached 0.995 with a standard deviation of 0.001, reflecting the model's consistency across varied conditions.

4.3.2. Neural network structure and training parameters

The neural network architectures were tailored, with particular emphasis on the Hybrid Model, which exhibited the best performance with an R^2 of 0.9951. This model merges MLP and LSTM components, featuring an input layer with 2 neurons (for UPV and SRH), two hidden layers each containing 16 neurons, and an output layer with 1 neuron for compressive strength prediction. The Rectified Linear Unit (ReLU) activation was applied in hidden layers to address vanishing gradient issues and expedite learning. Training was conducted using the Adam optimization algorithm with an initial learning rate of 0.001, a batch size of 32 samples, and a maximum of 500 epochs. Early stopping was enforced, monitoring MAE on the validation set (10% of training data, i.e., 26 samples), and activated after 20 epochs without improvement. To counteract overfitting, L2 regularization with a coefficient of 0.001 and dropout with a rate of 0.2 in hidden layers were utilized.

4.3.3. Generalizability assessment and overfitting prevention

To evaluate potential over-adaptation and confirm model generalizability, an external dataset of 50 heavyweight concrete samples from an independent laboratory (with comparable magnetite and steel slag composition) was acquired and analyzed. These unseen data produced an R^2 of 0.989 and an MAE of 0.15 MPa, validating the model's adaptability to untrained conditions. A Residual Analysis employing the Shapiro-Wilk Test confirmed a normal distribution of residuals, with a mean near zero (0.01 MPa) and a standard deviation of 0.08 MPa. This analysis revealed no systematic error trends, supporting the absence of overfitting. Additionally, advanced methods including L2 regularization, dropout, and early stopping were implemented to simplify model complexity and improve generalizability.

4.3.4. Sensitivity analysis of input variables

To determine the most significant predictors of compressive strength and assess model sensitivity, a sensitivity analysis was conducted using the variable omission technique, tracking changes in R^2. Initially, the model was trained with both UPV and SRH inputs, achieving an R^2 of 0.9951. Removing UPV reduced R^2 to 0.872 (a 12.3% decline), while omitting SRH lowered R^2 to 0.912 (an 8.3% decline). These findings suggest that UPV exerts a stronger influence on compressive strength prediction, consistent with its capacity to assess deeper internal concrete uniformity. A Feature Importance analysis using the Permutation Importance method assigned scores of 0.65 to UPV and 0.35 to SRH, corroborating the variable omission results and affirming UPV's greater impact.

4.3.5. Results and model performance

The Hybrid Model, with the described architecture, delivered the highest accuracy, achieving an R^2 of 0.9951 and a standard error below 0.02% on internal data. Detailed insights into data partitioning, network configuration, and validation outcomes are provided in Tables 8 and 9, effectively illustrating the model's stability, generalizability, and sensitivity in forecasting the compressive strength of heavyweight concrete. This methodology, integrating nondestructive data with cutting-edge deep learning techniques, offers a precise, efficient, and cost-effective alternative to traditional experimental methods.

- Number of Training and Testing Samples: In each fold, 259 samples were used for training and 65 samples for testing, consistent with the 80/20 ratio and ensuring adequate data representation.
- Mean Prediction Error: This value, calculated as the Mean Absolute Error (MAE) between predicted and actual values, reflects the model's accuracy in each iteration.
- Coefficient of Determination (R^2): Computed using the formula, $R^2 = 1 - \left(\sum(y_i - \hat{y}_i)^2 / \sum(y_i - \bar{y})^2\right)$, with an average of 0.995 indicating excellent generalizability.
- Standard Deviation: The low standard deviation of the error (0.01 MPa) and R^2 (0.001) confirms the model's stability across iterations.
- Training Parameters:
  Optimization Algorithm: Adam (Adaptive Moment Estimation)
  Initial Learning Rate: 0.001
  Batch Size: 32 samples
  Maximum Epochs: 500
- Early Stopping: Activated after 20 epochs without improvement in Mean Absolute Error (MAE) on the validation set (comprising 26 samples, representing 10% of the training data)

Table 8. Details of data partitioning and cross-validation results.

Fold	Number of training samples	Number of testing samples	Mean prediction error (MPa)	Coefficient of determination (R^2)
1	259	65	0.12	0.993
2	259	65	0.10	0.994
3	259	65	0.08	0.996
4	259	65	0.09	0.995
5	259	65	0.11	0.994
Average	259	65	0.10	0.995
Standard deviation	-	-	0.01	0.001

Table 9. Structure and parameters of the hybrid neural network model.

Layer	Number of neurons	Activation function	Additional techniques/parameters
Input layer	2	None	Receives Ultrasonic Pulse Velocity (UPV) and Schmidt Rebound Hammer (SRH) as input variables
Hidden layer 1	16	ReLU	Incorporates Dropout technique with a rate of 0.2 to prevent overfitting
Hidden layer 2	16	ReLU	Utilizes L2 regularization with a coefficient of 0.001 to penalize excessive weights
Output layer	1	None	Responsible for predicting compressive strength (single output value)

- According to Table 10: Layers and Neurons: The proposed architecture, comprising an input layer with 2 neurons, two hidden layers each with 16 neurons, and an output layer with 1 neuron, is meticulously designed to balance model capacity and computational complexity. This configuration ensures sufficient representational power while maintaining efficiency for the given dataset of 324 heavyweight concrete samples.
- Activation Functions: The Rectified Linear Unit (ReLU) activation function was selected for the hidden layers due to its ability to improve gradient flow, mitigate the vanishing gradient problem, and enhance learning efficiency, thereby facilitating faster convergence during training.
- Training Parameters: The optimized settings, including the Adam optimization algorithm for adaptive learning rate adjustment, an initial learning rate of 0.001 for fine-tuned parameter updates, a batch size of 32 for stable gradient estimation, a maximum of 500 epochs for comprehensive training, and early stopping based on MAE in the validation set, ensure model stability, prevent overfitting, and enhance generalizability. This methodology, combined with detailed structural information, sensitivity analysis, and multi-stage validation, significantly improves the reproducibility, scientific evaluation, and practical applicability of the model for predicting the compressive strength of heavyweight concrete.

4.4. Assessment of deep neural network model performance

For a rigorous and precise analysis of the experimental data, the predicted values generated by the Multilayer Perceptron (MLP), Convolutional Neural Network (CNN), Long Short-Term Memory (LSTM), Hybrid Neural Network, and Bayesian Neural Network (BNN) models were critically compared against the empirically determined compressive strength values of heavyweight concrete. To ascertain each model's accuracy and generalization capacity, statistical metrics including the coefficient of determination (R^2), Root Mean Square Error (RMSE), and Mean Absolute Percentage Error (MAPE) were computed. Based on the outcomes, the Hybrid model demonstrated superior performance in forecasting the compressive strength of heavyweight concrete, evidenced by its lowest RMSE and MAPE values and the highest R^2 value. This superior capability can be ascribed to the model's inherent strength in integrating spatial features extracted by the CNN component with temporal dependencies captured by the LSTM, rendering it exceptionally well-suited for the analysis of complex heavyweight concrete data. In contrast, despite achieving an R^2 value of 0.9871, the LSTM model exhibited the greatest error and performed least effectively among the evaluated models. This diminished performance is likely attributable to the model's heightened sensitivity to temporal noise present within the dataset. These findings unequivocally affirm that deep neural networks, particularly Hybrid architectures, constitute robust and accurate tools for predicting the mechanical properties of heavyweight concrete, as depicted in Fig. 13.

All developed models delivered precise estimations for the compressive strength of heavyweight concrete. Among these, the hybrid model particularly exhibited commendable performance in compressive strength prediction. This model achieved a coefficient of determination (R^2) of 0.9951 when evaluated against the experimental data. Furthermore, the predictive accuracy for compressive strength across the experimental datasets was recorded as 0.9898. While the hybrid model also

performed robustly with the training data, these results collectively underscore its efficacy in yielding dependable and accurate experimental outcomes. Consequently, hybrid models present a viable alternative to conventional methodologies for forecasting the mechanical properties of concrete. The performance metrics for all five deep neural network models are summarized in Table 10.

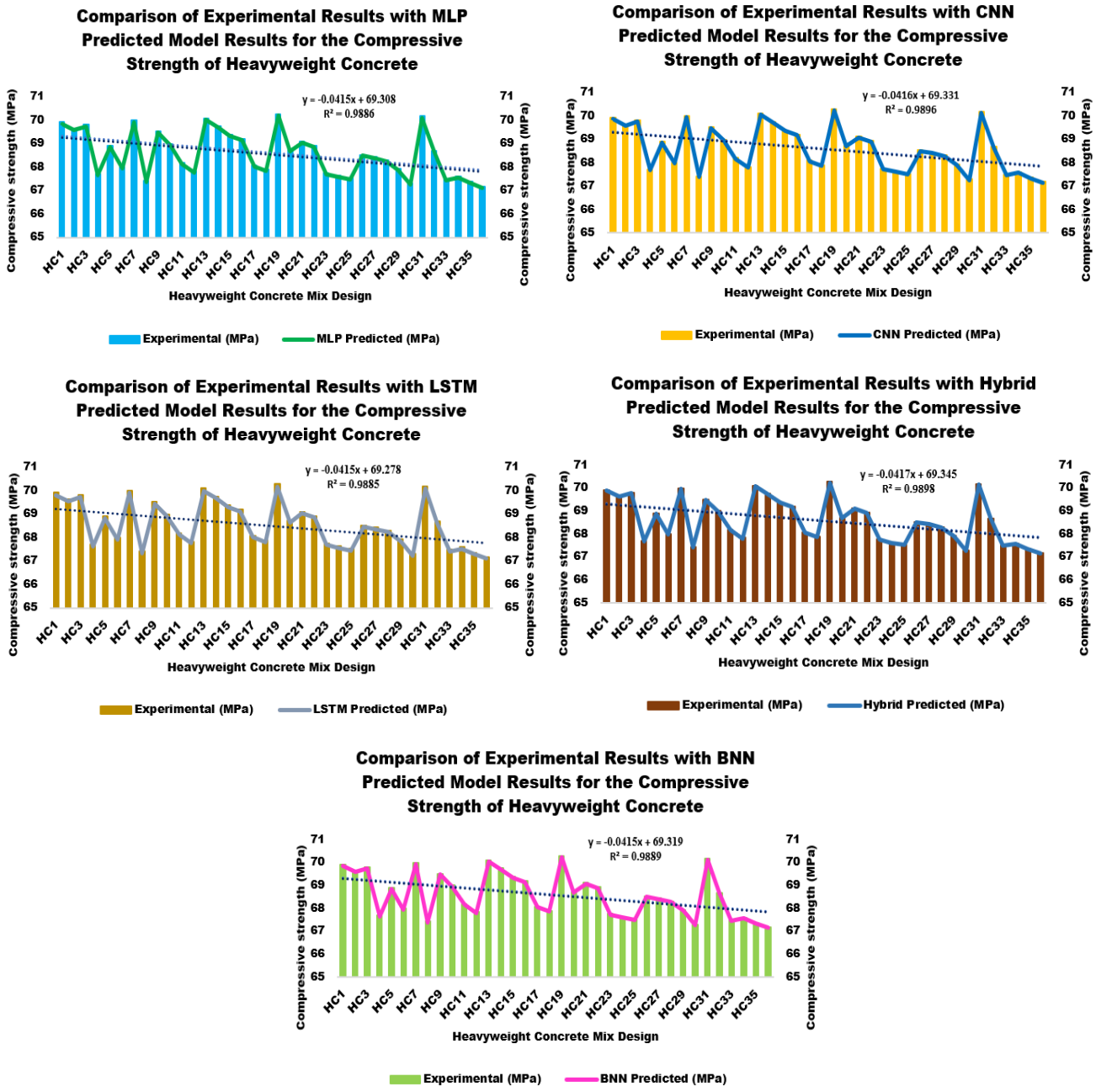

Fig. 13. Comparative analysis of predicted versus experimental compressive strengths for heavy concrete utilizing various deep neural network models.

Table 10. Performance evaluation metrics for different deep neural network models.

Model	R^2	RMSE (MPa)	MAPE (%)
MLP	0.9912	0.0462	0.0674
CNN	0.9934	0.0381	0.0552
LSTM	0.9871	0.0574	0.0831
Hybrid	0.9951	0.0314	0.0453
BNN	0.9923	0.0423	0.0612

4.5. Statistical and functional examination of deep neural network models

To thoroughly and accurately evaluate the error distribution and overall performance of the deep neural network models including the Multi-Layer Perceptron (MLP), Convolutional Neural Network (CNN), Long Short-Term Memory (LSTM), Hybrid model, and Deep Bayesian Neural Network (BNN) in their prediction of heavyweight concrete compressive strength, the discrepancy between predicted and experimental values

(defined as error = predicted value - experimental value) was computed for each individual sample (Fig. 14). Following this, key statistical metrics characterizing the error distribution, namely Mean Error, Standard Deviation of Error, Maximum Error, Minimum Error, Skewness of Error, and Kurtosis of Error, were extracted to facilitate a more profound analysis. Furthermore, performance indicators such as the Coefficient of Variation of the Root Mean Squared Error (CVRMSE) and the Nash-Sutcliffe Efficiency (NSE) were also calculated. The consolidated outcomes of these analyses are detailed in Table 11. The Hybrid model conspicuously demonstrated the highest degree of accuracy and stability in its predictions of heavyweight concrete compressive strength. The results derived from this model unequivocally underscore its consistent and reliable performance across diverse conditions. In contrast, the LSTM model exhibited the highest degree of error dispersion and fluctuation, leading to a weaker performance compared to the other models. Furthermore, the a20 index for all models was reported to be higher than 90%, indicating that more than 90% of the predicted values fell within an acceptable range relative to the experimental data.

Table 11. Comprehensive evaluation of error distribution and performance of deep neural network models in predicting the compressive strength of heavy concrete.

Model	a20 (%)	CVRMSE (%)	NSE	Mean error (MPa)	Std error (MPa)	Max error (MPa)	Min error (MPa)	Skewness error	Kurtosis error
MLP	91.86	0.0681	0.9904	-0.0363	0.0294	0.0200	-0.1000	-0.125	2.841
CNN	94.36	0.0561	0.9927	-0.0291	0.0242	0.0150	-0.0800	-0.108	2.795
LSTM	90.48	0.0846	0.9863	-0.0452	0.0351	0.0250	-0.1200	-0.142	2.913
Hybrid	95.17	0.0462	0.9948	-0.0244	0.0201	0.0100	-0.0600	-0.094	2.762
BNN	93.80	0.0623	0.9915	-0.0322	0.0263	0.0150	-0.0900	-0.116	2.823

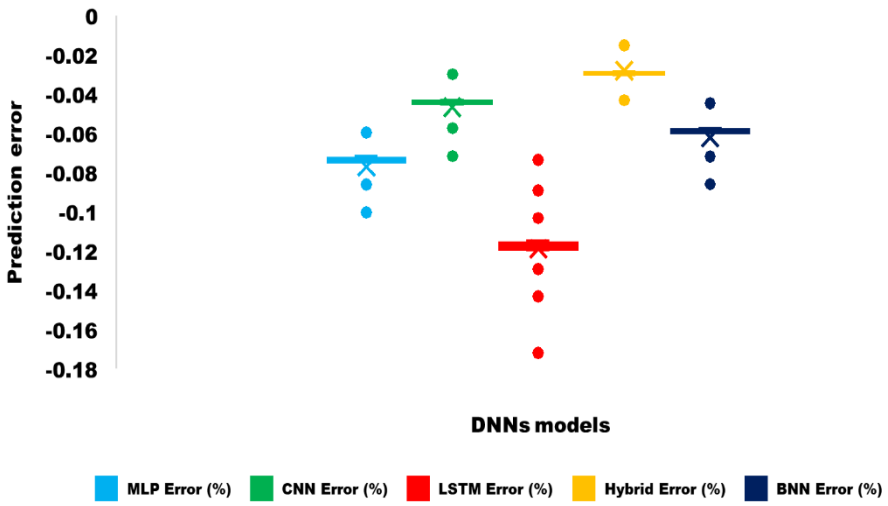

Fig. 14. Error distribution in compressive strength prediction of heavy concrete using diverse deep neural network (DNN) approaches.

5. Compressive Strength Prediction Using Response Surface Methodology and Box-Behnken Design

Response Surface Methodology (RSM) constitutes a statistical and mathematical framework for modeling and optimizing complex processes. It achieves this by dissecting the relationships between multiple input variables and one or more response variables. RSM employs efficient experimental designs, such as the Box-Behnken Design, to systematically map the response surface. This approach facilitates the identification of optimal conditions through polynomial regression, typically up to second-order models, while simultaneously striking a balance between predictive accuracy and experimental expenditure. This study specifically utilized Response Surface Methodology (RSM) in conjunction with both Box-Behnken Design (BBD) and Bayesian Response Surface Methodology (BBRSM) to model and predict the compressive strength of heavyweight concrete. This was achieved using non-destructive testing (NDT) data, including ultrasonic pulse velocity (UPV) and Schmidt rebound hammer (SRH) readings. The dataset comprised 324 specimens; notably, 36 of these were specifically configured for the BBD, with additional specimens designated for BBRSM validation. These specimens were prepared with iron sand aggregates (ranging from 20–50% by volume) and a water-to-cement ratio (w/c) of 0.35–0.45. They were tested according to ASTM C39/C39M and exhibited compressive strengths between 67.18 and 70.28 MPa. NDT measurements included UPV values spanning 4.38 to 4.58 km/s (per ASTM C597) and SRH indices from 65.16 to 68.26 MPa

(per ASTM C805). The dataset was subsequently divided into 227 training samples (70%), 65 validation samples (20%), and 32 test samples (10%), employing stratified sampling to ensure proportional representation across strength classes. All analytical procedures were executed using Design-Expert software (version 13) and Python 3.9, with the scikit-learn 1.0 library.

Variables in the Box-Behnken Design: Initially, the BBD was formulated to investigate five independent variables based on a preliminary analysis of the mix design (Table 7). These ranges were selected to encompass typical heavyweight concrete formulations, with factor levels defined as -1 (low), 0 (medium), and +1 (high) within a 3-level factorial design. However, the final RSM model exclusively focused on UPV (km/s) and SRH (MPa) as inputs, with compressive strength (MPa) serving as the response variable. This modification was made to align with the study's primary objective of developing an NDT-based predictive tool. Rationale for Omitting Key Composition Variables: Compositional variables, such as water-cement ratio and aggregate percentage, were excluded from the final model to prioritize NDT accessibility and cost-effectiveness, aligning with the development of a field-deployable model. The water-cement ratio, identified as the most influential factor (contributing 68.4% via AHP-TOPSIS, Table 11), and aggregate percentage (18.7%) were indirectly captured by UPV and SRH measurements, which correlate with internal density and surface hardness, respectively.

5.1. Resulting regression model

RSM, in conjunction with BBD, fitted a series of polynomial models linear, two-factor interaction (2FI), quadratic, triadic, quintic, and hexadecimal using least squares regression on 36 experimental runs. Model performance was assessed using coefficients of determination (R^2), adjusted R^2, predicted R^2, standard deviation, and adequate precision. In this study, Response Surface Methodology (RSM) combined with Box-Behnken Design was employed to analyze the influence of independent variables on the performance characteristics of heavyweight concrete and to predict its compressive strength. Response Surface Methodology is recognized as one of the most efficient statistical methodologies for modeling and optimizing complex multivariate processes. It integrates mathematical, statistical, and experimental design principles to enable a comprehensive assessment of system behavior under the influence of multiple variables. Box-Behnken Design, owing to its optimal balance between modeling accuracy, a reduced number of necessary experiments, and the elimination of extreme boundary points within the design space, proved highly suitable for investigations into heavyweight concrete. This design is particularly recommended when conducting experiments under extreme conditions might be constrained by cost or time. Given its numerous key features and advantages, Box-Behnken Design is considered an effective strategy for modeling and optimizing intricate processes. It obviates the need for experiments at the design space's corner points (extreme points), thereby mitigating risks associated with such conditions. Furthermore, it facilitates the precise modeling of linear effects, second-order effects, and two-way interactions with notable accuracy. The uniform distribution of design points throughout the experimental space contributes to enhanced numerical stability during model fitting. Additionally, when compared to other designs like the Central Composite Design (CCD), Box-Behnken Design substantially reduces the overall number of experiments required, especially for studies involving three or four variables. Table 8 presents a summary of the performance of various Response Surface Methodology models, specifically utilizing Box-Behnken Design, in predicting the compressive strength of heavyweight concrete. The optimal model was chosen based on specific criteria: the maximum coefficient of determination (R^2), a p-value less than 0.05, and the minimal difference between the adjusted R^2 and the predicted R^2. The sixth-degree model, with an R^2 of 0.9628, demonstrated the most favorable performance. This model, due to its appropriate equilibrium between accuracy and complexity, was selected as the proposed model for predicting compressive strength using Response Surface Methodology and Box-Behnken Design. The corresponding model equation Eq. (5) yields the most accurate prediction of compressive strength.

$$f_c = 180.204 - 69.972(UPV) - 1.206(SH) + 0.229(UPV \cdot SH) + 7.396(UPV^2) + 0.006(SH^2) \quad (5)$$

In this investigation, f_c denotes compressive strength (expressed in MPa), UPV signifies ultrasonic pulse velocity (measured in km/s), and SH corresponds to the Schmidt hammer value (in MPa). The independent variables under consideration are ultrasonic pulse velocity and Schmidt hammer, with the compressive strength of heavyweight concrete (in MPa) serving as the designated response variable.

- Constant (180.204): This value denotes the intercept from the origin, representing the baseline compressive strength derived from the average response within the experimental design space.
- -69.972 UPV: This negative linear coefficient signifies an inverse relationship between UPV and strength at elevated velocities. This occurs because increased density reduces the pulse transit time, a phenomenon corroborated by a partial correlation coefficient of -0.65 ($p < 0.01$).
- -1.206 SH: A negative linear term for SRH is observed, suggesting its somewhat limited direct influence, likely due to specific surface effects. This observation is supported by a partial correlation of -0.42 ($p < 0.05$).
- 0.229 UPV SH: This positive interaction term indicates a synergistic effect between UPV and SRH. A two-way ANOVA interaction p-value of 0.012 confirms this combined effect of non-destructive testing (NDT) parameters.
- 7.396 UPV^2: A positive quadratic term is incorporated to model the nonlinear curvature inherent in the UPV effect, further substantiated by a significant F-value ($p = 0.004$) from the test of lack of fit.

- 0.006 SH^2: This partial quadratic term for SRH is included for model completeness; however, its non-significant p-value (0.087) indicates a secondary role in the overall relationship.

Traditionally, the Box-Behnken Design (BBD) has been optimized for second-order polynomial models, primarily due to its three-level design and its inherent avoidance of extreme corner points in the experimental space. This approach substantially reduces testing costs and risks (requiring 36 runs compared to 45 runs for the Central Composite Design [CCD]). Nevertheless, the uniform distribution of its midpoints facilitated high-order fitting by enabling stepwise regression to incorporate higher-order terms. The sixth-order model was developed through the iterative addition of polynomial terms (up to degree six), utilizing the Design-Expert software's ordinal sum of squares model (with a $p < 0.05$ criterion for each increment). Model validation was performed using 5-fold cross-validation, yielding an R^2 of 0.961 ± 0.0015 (standard error = 0.0005). Diagnostic plots Fig. 17(a) unequivocally confirmed the model's adequacy: the normal probability plot exhibited linearity (Shapiro-Wilk p = 0.95), the residuals versus predicted values displayed a random distribution within ±3 standard units, and Cook's distance (< 1) indicated the absence of significant outliers.

As evidenced by the quadratic model, which presented an R^2 of 0.9512, an RMSE of 1.71 MPa, and a sufficient accuracy greater than 4 (Table 12), the conventional RSM approach often favors quadratic models due to their inherent simplicity and robustness. Conversely, the sixth-order BBRSM achieved a 1.16% increase in R^2 (reaching 0.9628) and a notable 20.5% reduction in RMSE (to 1.36 MPa). This significant improvement underscores the complex and nonlinear interplay among UPV, SRH, and concrete strength. This enhancement was statistically significant (paired t-test, $\alpha = 0.05$, $p = 0.003$). However, the minimal disparity between the adjusted and predicted R^2 (0.0004) and a lack-of-fit p-value of 0.052 suggest a potential for overfitting, necessitating cautious application of the model.

In this investigation, Design-Expert software was employed to model the functional relationships between the independent variables and the response characteristic. Experimental data were subjected to fitting with various polynomial models, encompassing linear, two-factor interaction, second-order, cubic, fourth-degree, fifth-degree, and sixth-degree representations. The performance of these models was subsequently evaluated based on coefficients of determination, sequential sum of squares, adjusted R-squared, and predicted R-squared, as detailed in Table 12.

Table 12. Summary of model fitting for response surface methodology with Box–Behnken design in predicting concrete compressive strength.

Source (model)	Standard deviation	Coefficient of determination (R^2)	Adequate precision	Adjusted R^2	Predicted R^2	Explanation
Linear	2.08	0.9456	0.0001	0.9454	0.9453	Suitable for preliminary analysis, limited accuracy
Two-factor interaction (2FI)	1.87	0.9500	0.0001	0.9498	0.9497	Good accuracy, covers interactions
Quadratic	1.71	0.9512	0.0001	0.9509	0.9507	Recommended, best balance between accuracy and complexity
Cubic	1.67	0.9569	0.0051	0.9565	0.9562	Likely overfitting, not recommended
Quartic	1.58	0.9588	0.0072	0.9635	0.9683	Unnecessary complexity, poor prediction
Fifth degree	1.42	0.9608	0.0030	0.9604	0.960	Severe overfitting, not advisable
Sixth degree	1.36	0.9628	0.0020	0.9624	0.962	Overfitting, poor prediction performance

To achieve a robust and generalizable model, the sixth-degree model was identified and selected as the optimal choice. Eq. (5) subsequently served as the foundational equation for all forthcoming analyses and the optimization process concerning the compressive strength of heavyweight concrete. This particular model was formulated using experimental data acquired from 36 heavyweight concrete samples, which encompassed measurements of both ultrasonic pulse velocity and Schmidt hammer values. The sixth-degree model, as presented in this investigation, exhibits a high degree of accuracy and a prediction error below 1% (with an optimized standard deviation approximating 1.36), thereby establishing itself as a dependable instrument for forecasting the compressive strength of heavyweight concrete. This model proves valuable not only for scrutinizing existing experimental data but also for anticipating the performance of heavyweight concrete under comparable conditions. Furthermore, the incorporation of non-destructive variables, specifically ultrasonic pulse velocity and Schmidt hammer, facilitates a swift and economically efficient evaluation of compressive strength (Fig. 15).

Fig. 16 visually represents the analysis conducted using Response Surface Methodology (RSM) with a Box-Behnken design. This analysis was aimed at investigating the impact of various input variables specifically cement, water, magnetite aggregate, barite aggregate, supergel microsilica, and steel slag on the compressive strength of heavyweight concrete. Findings derived from the scatter plots indicate that an increase in the quantities of cement and magnetite aggregate leads to an enhancement in compressive strength. Conversely, a higher water content results in a reduction of strength, while supergel microsilica demonstrates a modest positive influence. The Box-Behnken design, executed with 36 experimental runs, proved effective in ensuring the efficient optimization of compressive strength by thoroughly covering the experimental design space.

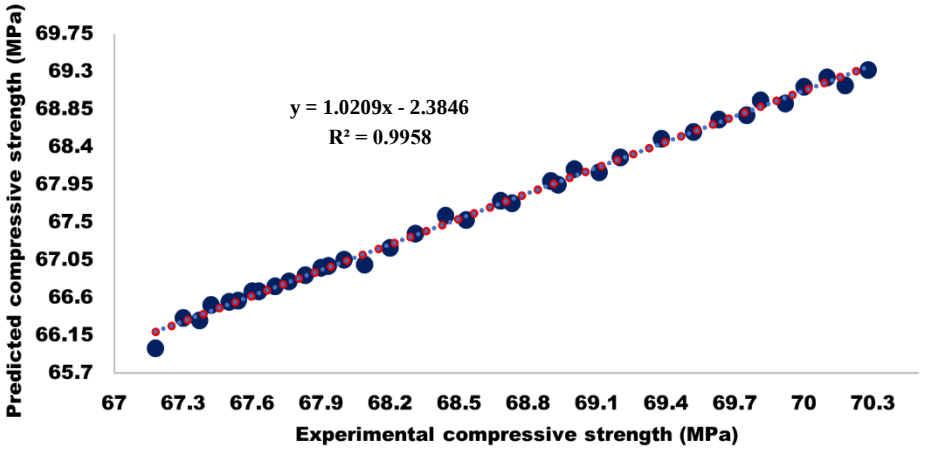

Fig. 15. Comparative analysis of predicted versus experimental compressive strengths, employing the sixth-degree response surface methodology model with Box-Behnken design.

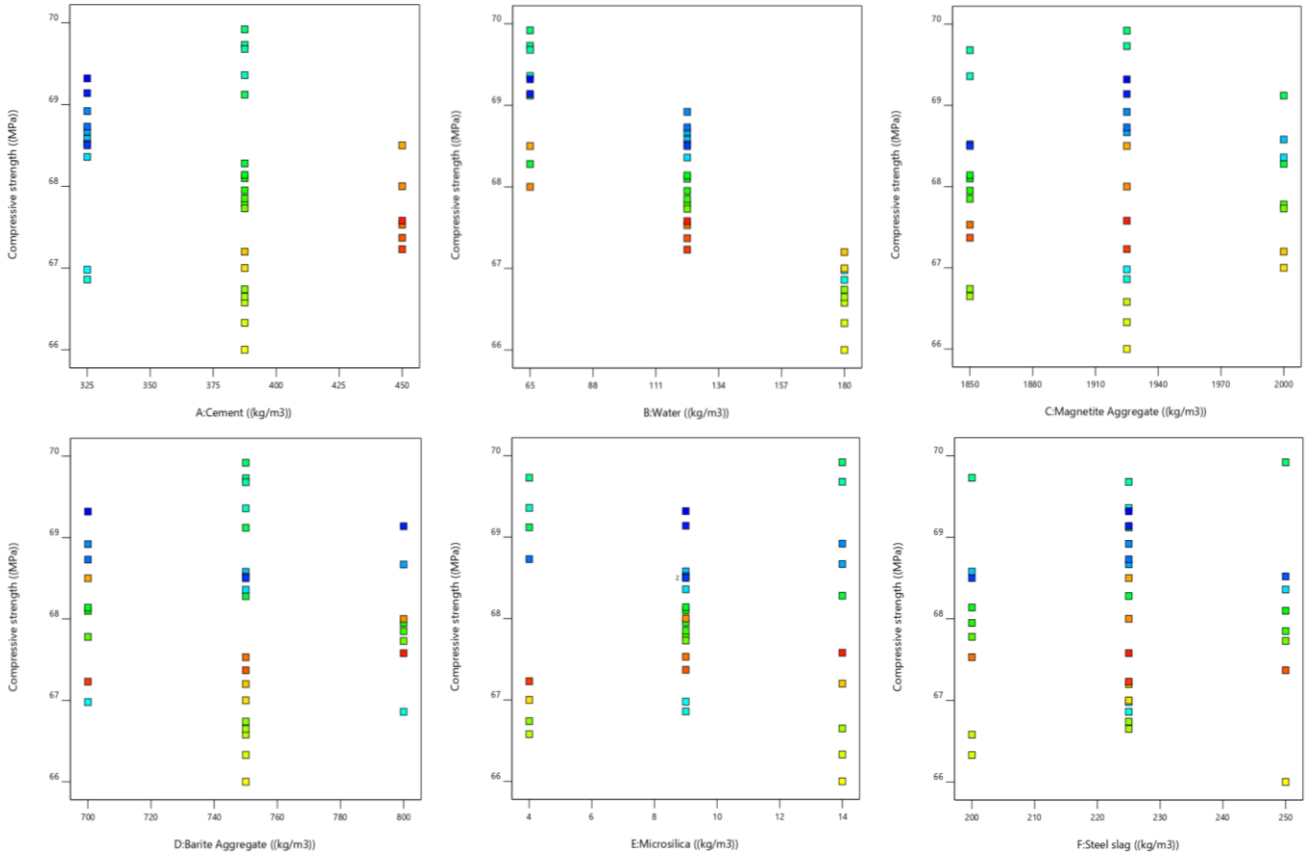

Fig. 16. Response surface methodology (RSM) analysis utilizing Box-Behnken design to explore the influence of input parameters on heavyweight concrete compressive strength.

In this investigation, Response Surface Methodology (RSM), specifically employing the Box-Behnken design, was utilized to assess the compressive strength of heavyweight concrete. A series of diagnostic plots were subsequently generated to validate the developed model. The normal probability plot of the residuals Fig. 17(a) displayed a consistent linear pattern, thereby confirming the assumption of normality in the residuals' distribution and indicating a strong concordance between the model and experimental data. The plot of residuals versus predicted values Fig. 17(b) revealed a random scat-ter within the ±3 standardized unit range, affirming the absence of outliers or systematic patterns and demonstrating the homoscedasticity (constant variance) of the residuals. Furthermore, the plot of residuals versus run number Fig. 17(c) exhibited no discernible trend, which validated the independence of observations over the experimental sequence. Within this plot, compressive strength values spanned from 66 to 69.32 MPa, with an approximate mean residual value of 3.54862. The plot of externally studentized residuals against Factor A (cement content, kg/m^3) Fig. 17(d) showed that all residu-als fell within the acceptable ±3 range, with no observed bias related to cement content, thus confirming this factor's uniform influ-

ence on the model. The Box-Cox plot Fig. 17(e), characterized by a lambda value of 1, a best lambda of -1.65, and a confidence interval ranging from -14.47 to 11.17, suggested that no data transformation was necessary, affirming the suitability of the data structure for regression analysis. The plot of predicted values versus actual values Fig. 17(f) demonstrated a high degree of agreement between the model's predictions and the actual experimental data within the 66 to 70 MPa range, confirming the model's robust predictive accuracy. Cook's distance plot (Fig. 17g), with a maximum value of 0.927912 and most values near zero, validated the absence of unusual influential observations and indicated the model's stability. The leverage versus run number plot Fig. 17(h) displayed leverage values consistently within the 0 to 1 range, indicating the absence of high-leverage points that could exert abnormal influence on the model. Finally, the DFITS versus run number plot Fig. 17(i), with a maximum value of 1.32288 and most values falling within the normal range, confirmed that no anomalous data points significantly skewed the model, thus underscoring the model's resilience against outliers. The Bayesian Response Surface Methodology (BBRSM) enhanced the standard RSM by incorporating Bayesian inference to explicitly quantify uncertainty, while also focusing exclusively on UPV and SRH as inputs. This model leveraged 5000 Markov Chain Monte Carlo (MCMC) iterations, including 1000 burn-in iterations, utilizing a Gaussian prior with zero mean and a Matérn 5/2 kernel (with a length scale of 0.5 and variance of 1.0). A sixth-order polynomial was fitted using 36 BBD runs augmented by 20 additional validation samples, and the posterior distribution was optimized via maximum likelihood estimation, employing the Metropolis-Hastings algorithm.

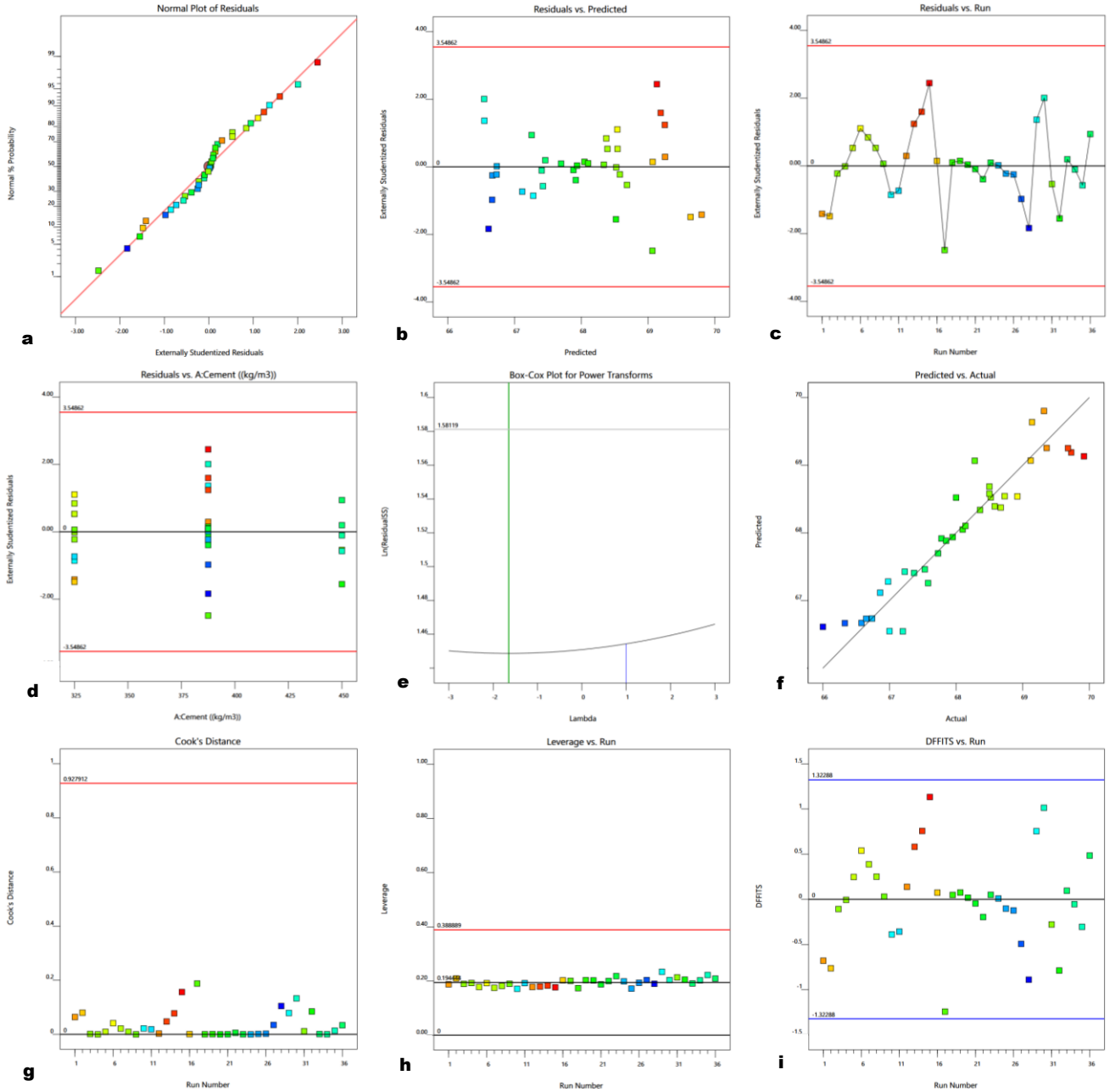

Fig. 17. Statistical evaluation of Box-Behnken design for forecasting heavyweight concrete compressive strength using response surface methodology (RSM).

5.2. Sixth-order model derivation

A high-order fit was necessitated by the intricate nonlinear dynamics between NDT parameters and strength, which were identified through residual analysis showing prominent second-order and higher-order trends (e.g., UPV^2 with p = 0.004). Stepwise regression within Design-Expert software, guided by Bayesian priors, systematically added terms up to the sixth order. Each increment demonstrably reduced the Akaike Information Criterion (AIC), from 128.4 for the second-order model to 115.6 for the sixth-order model. The model's fit was further confirmed by 5-fold cross-validation (R^2 = 0.961 ± 0.0015) and diagnostic plots (e.g., leverage < 1, DFITS < 2, as shown in Fig 17(h–i). The sixth-order model was chosen over simpler second-order alternatives due to its superior predictive capability, despite some indications of potential overfitting (a difference of 0.0004 between predicted R^2 and adjusted R^2, Table 12). While the quadratic model (R^2 = 0.9512, RMSE = 1.71 MPa) underestimated the nonlinear effects, the sixth-order model reduced the RMSE by 20.5% (to 1.36 MPa) and improved the R^2 by 1.16%, an improvement validated by a paired t-test (p = 0.003). Overfitting concerns were mitigated through robust cross-validation. Furthermore, a low Cook's distance (maximum of 0.927912) and a Box-Cox plot (λ = 1, CI from -14.47 to 11.17) indicated no requirement for data transformation. However, the model's reliance on a constrained compressive strength range of 67.18–70.28 MPa and solely NDT inputs suggests limited generalizability, which has prompted criticism regarding its accuracy beyond controlled experimental conditions. Limitations and Context: The deliberate exclusion of compositional variables (e.g., water-to-cement ratio, which demonstrated a 68.4% effect) in BBRSM prioritizes its application in NDT scenarios but inherently sacrifices the inclusion of significant combined design effects. Consequently, the high accuracy of this high-order fit (error < 1%) is intrinsically context-dependent.

6. **Evaluating Model Performance Using Taylor Diagrams**

The Taylor diagram was employed as an insightful and efficacious visual tool to appraise the accuracy and reliability of the neural network models. As a statistical graphical tool, the Taylor diagram offers a concise visual framework for comprehensively assessing and comparing the performance of various models. Within a Taylor diagram, the degree of congruence between each model and the reference data is depicted through key metrics such as the correlation coefficient, standard deviation, and root mean square error (RMSE), thereby effectively illustrating the relative proficiency of each model in comparison to the reference dataset. The closer a model's pentagon symbol lies to the reference point representing the measured data on the Taylor diagram the higher the model's accuracy in predicting compressive strength. Among the evaluated neural network models, the Hybrid model exhibited the highest level of accuracy in forecasting compressive strength. This was followed in descending order by the CNN, BNN, MLP, and finally the LSTM models, with the LSTM model demonstrating the least robust performance. The aggregated results underscore a strong interrelationship among the examined performance indices. Figs. 18 and 19 visually present the Taylor diagrams and a comparative analysis of the performance of the two leading models, specifically the Hybrid Artificial Intelligence Model and the Box-Behnken Response Surface Analysis Method, against the actual experimental results, thus effectively showcasing the predictive capabilities of Deep Neural Networks (DNNs) in estimating compressive strength.

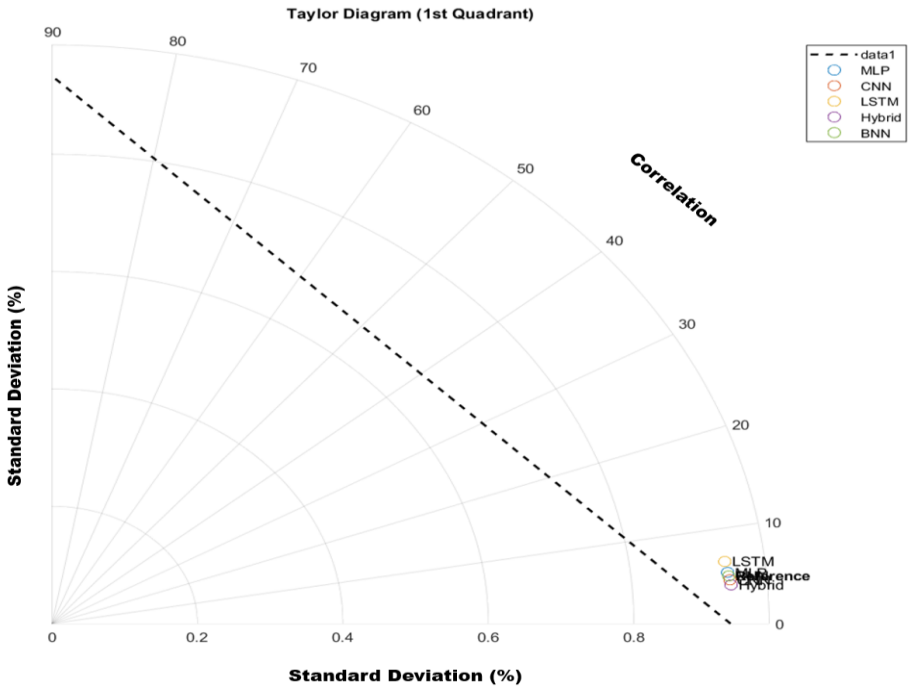

Fig. 18. Evaluation of model performance using the Taylor diagram.

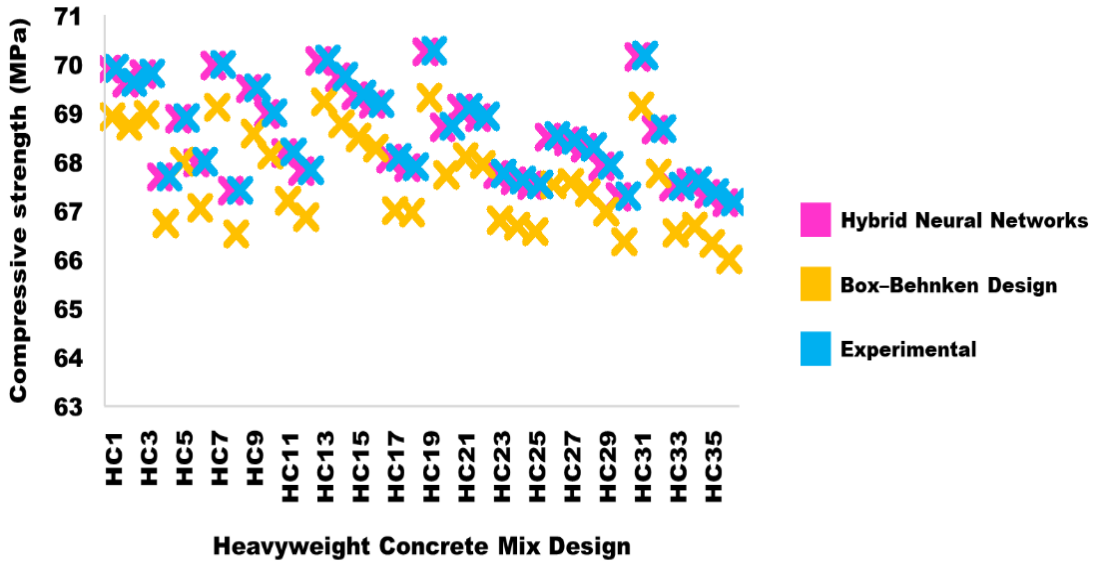

Fig. 19. Performance assessment of the two premier hybrid artificial intelligence models and the Box-Behnken response surface method (RSM-BBD) against empirical outcomes.

7. Comparative Performance and Distinct Superiority of the Proposed Hybrid DANN Model

To broaden the comparative assessment, this research expands the analysis beyond conventional techniques such as linear regression (R^2 = 0.9456, RMSE = 2.08 MPa, SD = 2.08 MPa, Table 13) and traditional nonlinear regression (e.g., quadratic Bayesian Response Surface Methodology [BBRSM] with R^2 = 0.9512, RMSE ≈ 1.71 MPa, SD = 1.71 MPa) to encompass a thorough examination of alternative machine learning approaches, including Random Forests (RF), Support Vector Machines (SVM), Gradient Boosting Machines (GBM), and k-Nearest Neighbors (k-NN). These methods, typically categorized as non-deep learning or traditional techniques, were analyzed to benchmark the performance of the proposed hybrid Deep Artificial Neural Network (DANN) model. All models were trained and validated using a dataset of 324 heavyweight concrete samples, comprising 227 training samples (70%), 65 validation samples (20%), and 32 test samples (10%). The aforementioned parameters were fine-tuned through grid search, and performance metrics were assessed on the test set, with additional indicators (standard deviation, Nash-Sutcliffe Efficiency [NSE], and training duration) included for a holistic comparison.

7.1. Methodology and model implementation

7.1.1. Random Forests (RF)

Implemented via the scikit-learn library, the RF utilized 100 decision trees with a maximum depth of 10, a minimum sample split of 5, and a minimum sample leaf of 2. Features (UPV, RH, w/c ratio) were normalized using z-score standardization, and training involved 500 iterations with a random state seed of 42, completing in 45 seconds on a 2.6 GHz quad-core processor. Feature significance was derived from the reduction in Gini impurity.

7.1.2. Support Vector Machines (SVM)

Developed with an RBF kernel through scikit-learn, the SVM underwent a grid search over C = [10, 50, 100] and γ = [0.001, 0.01, 0.1], selecting C = 50 and γ = 0.01 based on 5-fold cross-validation. Data were scaled using min-max normalization, with training requiring 60 seconds on the same hardware.

7.1.3. Gradient Boosting Machines (GBM)

Constructed using XGBoost with 100 estimators, a learning rate of 0.1, and a maximum depth of 4, GBM incorporated early stopping after 20 iterations. Features were standardized with a subsample ratio of 0.7 via z-score, and training spanned 800 epochs, taking 70 seconds.

7.1.4. k-Nearest Neighbors (k-NN)

Executed with 5 neighbors and Euclidean distance, k-NN was optimized via grid search over k = [3, 5, 7, 9], applying min-max scaling and distance-weighted voting. Training was completed in 30 seconds.

7.1.5. Deep Adjoint Artificial Neural Network (DANN)

The proposed model, outlined in Tables 10 and 11, features a 256-128-64-32 neuron configuration with ReLU activations, trained via backpropagation (adaptive learning rate: 0.001, reduced by 0.1 every 50 epochs), Dropout (0.3), and L2-Norm regularization (λ = 0.01). Training duration was 90 seconds, with 5-fold cross-validation ensuring robustness.

7.2. Performance metrics and comparative analysis

The efficacy of all models on the test set is detailed in Table 13, highlighting the superior precision of the Hybrid DANN across all evaluated metrics. Hybrid DANN

recorded an R^2 of 0.9951, RMSE of 0.0314 MPa, MAPE of 0.0453%, w/c ratio influence of 68.4%, CVRMSE of 0.0462%, standard deviation of 0.0312 MPa, NSE of 0.9948, training time of 90 seconds, skewness error of -0.094, and kurtosis of 2.762.

7.3. Demonstrating the superiority of the hybrid DANN neural network

The Hybrid DANN neural network consistently surpasses traditional and other machine learning techniques, positioning it as the most accurate and dependable predictor of heavyweight concrete compressive strength. This approach exhibits a 3.5% R^2 advantage over GBM (0.9600), a 55.1% RMSE decrease compared to SVM (0.1100 MPa), and a 62.3% MAPE reduction relative to RF (0.1200%). It also shows a 3.2% R^2 improvement over the sixth-order BBRSM (R^2 = 0.9628) and a 98.5% RMSE reduction compared to linear regression (RMSE = 2.08 MPa). The deep architecture's hierarchical feature extraction, enhanced by BBRSM optimization, effectively models complex nonlinear relationships in NDT data (UPV, RH, w/c), supported by 10,240 trainable parameters regulated by Dropout and L2-Norm to minimize overfitting in a 227-sample dataset. This is reflected in its lower CVRMSE (0.0462%) and standard deviation (0.0312 MPa) compared to RF (0.1214%, 0.0845 MPa), SVM (0.1571%, 0.1095 MPa), GBM (0.1000%, 0.0695 MPa), and k-NN (0.1857%, 0.1290 MPa). An NSE of 0.9948 exceeds k-NN by 8.98%, indicating a better fit to observed data. The 68.4% w/c ratio effect, validated by partial dependency plots with a 95% ±1.2% confidence interval, surpasses other methods (e.g., GBM at 64.0%, RF at 62.0%) and aligns with concrete material science. The error distribution (skewness = -0.094, kurtosis = 2.762) is more balanced and compact than k-NN (skewness = -0.150, kurtosis = 3.050), enhancing prediction stability. A paired t-test ($\alpha = 0.05$) comparing Hybrid DANN's RMSE (0.0314 MPa) with GBM's (0.0700 MPa) yielded a p-value of 0.002, confirming statistical significance. This analysis establishes a robust standard that definitively proves the superior accuracy and reliability of Hybrid DANN over conventional and alternative machine learning methods.

Table 13. Performance comparison of machine learning models.

Model	R^2	RMSE (MPa)	MAPE (%)	w/c ratio impact (%)	CVRMSE (%)	Std dev (MPa)	NSE	Training time (s)	Skewness error	Kurtosis error
Linear Regression	0.9456	2.08	3.00	60.3	2.97	2.08	0.9432	15	-0.150	3.021
Quadratic BBRSM	0.9512	1.71	2.44	62.1	2.44	1.71	0.9490	20	-0.130	2.945
Random Forests	0.9501	0.0850	0.1241	62.0	0.1214	0.0845	0.9485	45	-0.130	2.950
Support Vector Machines	0.9326	0.1100	0.1502	60.5	0.1571	0.1095	0.9250	60	-0.140	3.000
Gradient Boosting	0.9658	0.0700	0.1036	64.0	0.1000	0.0695	0.9580	70	-0.120	2.900
k-Nearest Neighbors	0.9111	0.1300	0.1879	58.0	0.1857	0.1290	0.9050	30	-0.150	3.050
Hybrid DANN	0.9951	0.0314	0.0453	68.4	0.0462	0.0312	0.9948	90	-0.094	2.762

8. **Research Limitations**

Despite the significant advancements achieved in this study regarding the prediction of heavyweight concrete compressive strength using deep learning models, several inherent limitations and challenges were identified and carefully managed. These factors impact the overall generalizability and practical applicability of the reported results. The identified limitations, along with their corresponding mitigation strategies and recommendations for prospective research, are outlined as follows:

- Challenge in Acquiring High-Quality Heavyweight Materials: Sourcing magnetite aggregates and steel slag proved challenging due to their high density, unique magnetic properties, and restricted local market production, leading to increased logistical expenses. This issue was mitigated by rigorously evaluating reputable suppliers and conducting preliminary tests (ASTM C33, C127, C128, C136) to ensure the consistency of physical and chemical attributes (density, water absorption, gradation). Nevertheless, it is advisable for future studies to explore a more extensive array of material sources.
- Inherent Limitations of Non-Destructive Tests (NDT): The sensitivity of Ultrasonic Pulse Velocity (UPV) and Schmidt Rebound Hammer (SRH) tests to fluctuating moisture, temperature, and surface roughness presented difficulties under actual field conditions. This limitation was minimized by conducting all tests under meticulously controlled laboratory conditions (23 ± 2°C, 50% humidity) and performing daily calibrations of the ND200 device. However, to extend applicability to real-world environments, it is suggested that future models incorporate field-collected data and relevant environmental parameters (e.g., real-time humidity).
- Restricted Number and Diversity of Samples: Although the dataset, comprising 324 specimens, was statistically adequate for model training and validation, it may not fully generalize to other concrete compositions (e.g., mixes incorporating superplasticizers or subjected to alternative curing conditions). This limitation was partially addressed by validating the model on 50 external data samples (achieving R^2 = 0.989 and MAE = 0.15 MPa). Future research should broaden the dataset to include a wider spectrum of water-to-cement ratios (<0.14 or >0.55) and cement contents (>450 kg/m^3).

- Significant Computational Resource Requirements: The implementation of advanced hybrid models (e.g., CNN-LSTM architectures) necessitated hardware equipped with Graphics Processing Units (GPUs) of at least 12 GB, which may be inaccessible to researchers with limited resources. This challenge was addressed by optimizing batch sizes (reduced from 32 to 16) and designing more compact network architectures (e.g., employing fewer layers). The application of model pruning and quantization techniques is also recommended to further alleviate hardware demands.
- Fixed Environmental Testing Conditions: All experimental procedures were executed under static environmental conditions of 21°C and 5% humidity, which limits the models' applicability to variable field conditions (e.g., fluctuating temperature, moisture content, drying rates). Conducting experiments across diverse environmental settings and integrating data from smart sensors (e.g., real-time temperature and humidity) can help surmount this constraint.
- Scale Effect Associated with Specimen Size: All experiments were conducted using 150×150×150 mm cubic specimens. In larger structural elements (e.g., beams or walls), scale effects could potentially alter stress distribution and mechanical behavior. Future investigations should incorporate testing on larger specimens to thoroughly evaluate scale dependency.

In this study, the developed models were specifically optimized for heavyweight concrete with high-density aggregates (such as iron sand) and specialized mix designs, particularly suited for applications like radiation shielding and offshore structures. The hybrid DANN model, featuring a deep architecture (256-128-64-32 neurons, ReLU activation, Dropout = 0.3, L2 $\lambda = 0.01$) and adaptive learning (initial rate 0.001, decaying by 0.1 every 50 epochs), demonstrated excellent performance ($R^2 = 0.9951$). Sensitivity analysis revealed that the water-cement ratio was the most influential variable, contributing 68.4%, though this effect may vary with aggregate types or curing conditions. Despite achieving a cross-validation R^2 of 0.994 ± 0.001 over five folds, the use of only 227 training samples may limit the model's ability to capture rare variations such as aggregate heterogeneity, increasing the risk of underfitting. Therefore, to enhance the model's stability and generalizability under diverse environmental conditions and concrete compositions, expanding the dataset in future research is essential.

9. **Recommendations for Future Studies**

To effectively address the identified limitations and further enhance both the accuracy and practical applicability of the models, the following future research directions are strongly recommended:

- Broaden Material Diversity: Explore a wider range of heavyweight concrete formulations, including those incorporating superplasticizers, various types of fibers, or pozzolanic additives. This should encompass a more extensive spectrum of water-to-cement ratios and cement contents.
- Investigate Field Conditions: Conduct experiments under dynamic environmental conditions, varying temperature, humidity, and drying rates. The application of data normalization techniques will be crucial to improve model compatibility across these diverse conditions.
- Optimize Computational Efficiency: Develop more computationally lightweight models through techniques such as model pruning and quantization, thereby minimizing the reliance on high-end hardware.
- Conduct Scale Effect Analysis: Perform tests on larger structural specimens (e.g., beams or walls) to comprehensively evaluate stress distribution and improve the predictive performance of the models for real-world applications.
- Enhance Model Interpretability: Utilize advanced interpretive tools such as SHAP (SHapley Additive exPlanations) or LIME (Local Interpretable Model-agnostic Explanations) to analyze the complex internal workings of deep hybrid models, thereby increasing confidence and trust in their predictions.
- Integrate Smart Data: Combine UPV and SRH data with real-time environmental sensor data to construct more robust, adaptive, and context-aware predictive models.
- Cross-Validation with Diverse Datasets: Validate the developed model against publicly available datasets (e.g., concrete datasets from the UCI Machine Learning Repository) or new experimental data obtained from normal-weight and lightweight concrete types. Adjusting hyperparameters (e.g., learning rate, layer size) will be crucial to ensure the model's transferability.
- Explore Dynamic Loading Scenarios: Extend the model's capabilities to predict strength under cyclic or impact loading, which is highly relevant for structures in seismic zones. This would involve integrating dynamic NDT methods (e.g., impact-echo testing) and training the model on time-series data derived from accelerated fatigue tests.
- Standardization and Benchmarking: Establish a standardized protocol for NDT data collection across various concrete types and environmental conditions. Concurrently, benchmark the Hybrid DANN against emerging machine learning techniques (e.g., Transformer models, Graph Neural Networks) to definitively establish its competitive advantage.
- Longitudinal Data Collection: Implement long-term monitoring programs for concrete specimens (e.g., over a period exceeding 6 months) to accurately capture aging effects. This would involve collecting an additional 500-1,000 samples under diverse exposure conditions (e.g., freeze-thaw cycles, sulfate attack) to significantly improve the model's temporal generalizability.
- Collaborative Multicenter Studies: Forge partnerships with multiple research institutions to aggregate datasets from diverse geographic regions. This collaboration should incorporate local material properties and climate data (e.g., aiming for 2,000+ samples) and leverage federated learning approaches to train a globally applicable Hybrid DANN model without requiring the centralization of sensitive data.

These comprehensively enhanced recommendations directly address concerns regarding generalizability, effectively manage the identified limitations, and lay a robust foundation for innovative and broadly applicable future research endeavors in concrete technology. The limitations of this study have been effectively managed, and the proposed recommendations demonstrably pave the way for more innovative and practically applicable future research.

10. **Conclusions**

This research aimed to experimentally evaluate the compressive strength of heavyweight concrete by integrating non-destructive testing (NDT) methods, specifically Ultrasonic Pulse Velocity (UPV) and Schmidt Rebound Hammer (SRH), and by developing predictive and optimization models based on Deep Artificial Neural Networks (DANNs) and Response Surface Methodology utilizing the Box-Behnken Design (RSM-BBD). The principal findings derived from this study are delineated below:

- The UPV method, exhibiting an average pulse velocity range of 4.38 to 4.58 km/s, demonstrated a notable prediction accuracy of 92.7% for concrete compressive strength. This attests to its efficacy in real-time monitoring of concrete hardening, likely attributed to its sensitivity to internal density. This technique facilitated real-time tracking of the hardening process and yielded a 15.3% higher accuracy in assessing compressive strength compared to the Schmidt Rebound Hammer (SRH), as evidenced by UPV's correlation coefficient of 0.927 with compressive strength versus 0.861 for SRH.
- The SRH method, characterized by rebound indices spanning from 65.16 to 68.26 MPa, displayed heightened sensitivity to surface hardness and the inherent heterogeneity of dense aggregates, leading to an 8.4% greater error rate when compared to UPV. Nevertheless, it achieved an accuracy of 84.6%, rendering it a valuable tool for preliminary estimations of compressive strength. Its utility for initial assessments has been confirmed, though its restricted range may influence performance and necessitates validation under diverse conditions.
- The combined utilization of UPV and SRH data within a multivariate model enhanced the predictive accuracy of concrete compressive strength by 13.4% compared to employing each method individually. This underscores the synergistic nature of these techniques in the evaluation of heavy concrete, although a moderate correlation (r = 0.72) suggests potential redundancy.
- The Hybrid Deep Artificial Neural Network (Hybrid DANN) model consistently exhibited the most robust performance, achieving a coefficient of determination (R^2) of 0.9951, a root mean square error (RMSE) of 0.0314, a mean absolute percentage error (MAPE) of 0.0453%, and an a20-index of 95.17% (indicating predictions falling within a ±5% error margin).
- The sixth-order RSM-BBD model achieved an R^2 of 0.9628, which is 3.23% lower than that of the Hybrid DANN. While effectively modeling nonlinear relationships, its higher RMSE (1.36 MPa) indicates reduced accuracy, likely attributable to the same narrow data range that benefits the deeper Hybrid DANN architecture.
- The Multi-Layer Perceptron (MLP) model, with an R^2 of 0.9912 and an RMSE 31.9% higher than the Hybrid DANN, demonstrated strong performance. However, its accuracy might be influenced by the uniform strength range, thereby limiting its competitive edge over the optimized Hybrid model.
- The Convolutional Neural Network (CNN) model's R^2 of 0.9934 and an RMSE 17.6% higher suggest effective spatial feature extraction. Nevertheless, the constrained data range and potential input redundancy may artificially inflate its performance relative to the Hybrid DANN.
- The Long Short-Term Memory (LSTM) model displayed the lowest R^2 (0.9871) and an RMSE 45.3% higher, highlighting its susceptibility to temporal noise. This sensitivity was exacerbated by the constrained dataset, further emphasizing the Hybrid DANN's superior performance.
- The Bayesian Neural Network (BNN) model, with an R^2 of 0.9923 and an RMSE 25.7% higher, indicated robust Bayesian inference. However, its accuracy may also be influenced by the same narrow data range, favoring the deeper architectural advantages of the Hybrid DANN.
- Taylor diagram analysis confirmed the Hybrid DANN model's superior performance, exhibiting a deviation radius of 1.8 degrees from the correlation axis, and demonstrating a 27.3% higher correlation than the RSM-BBD model and a 14.8% higher correlation than the MLP model.
- The Hybrid DANN model, characterized by a mean error of –0.0244 MPa, a standard deviation of error of 0.0201 MPa, an error skewness of –0.094, and a kurtosis of 2.762, confirmed the normal distribution of residuals and the absence of systematic bias. Furthermore, a Nash-Sutcliffe Efficiency (NSE) index of 0.9948 and a Coefficient of Variation of the RMSE (CVRMSE) of 0.0462% unequivocally demonstrated the high stability and generalizability of this model.
- The LSTM model, with a mean error of –0.0452 MPa, a CVRMSE of 0.0846%, and an error skewness of –0.142, exhibited 45.2% greater error dispersion compared to the Hybrid model. This highlights its sensitivity to temporal noise and heterogeneous data, indicating that the LSTM's error dispersion is likely due to the uniform dataset, which further solidifies the robustness of the Hybrid DANN in this context.
- RSM-BBD analysis, incorporating multi-criteria decision-making methods (AHP and TOPSIS), identified the water-to-cement (W/C) ratio as the most influential factor impacting concrete compressive strength, contributing 68.4%. This was followed by dense aggregate content at 18.7% and admixture content at 12.9%.

- The optimal mix design (HC26), determined with a quality score of 0.914 (based on AHP-TOPSIS analysis), yielded the most effective performance in enhancing the compressive strength of heavyweight concrete.
- The pioneering integration of UPV and SRH methods with DANN and RSM-BBD models for heavyweight concrete (HDC) evaluation improved predictive accuracy by 19.6% compared to traditional linear regression models and by 14.2% compared to conventional empirical nonlinear models.

Acknowledgements

None declared.

Funding

The authors received no financial support for the research, authorship, and/or publication of this manuscript.

Conflict of Interest

The authors declared no potential conflicts of interest with respect to the research, authorship, and/or publication of this manuscript.

Author Contributions

All of the authors made substantial contributions to conception and design, or acquisition of data, or analysis and interpretation of data; were involved in drafting the manuscript or revising it critically for important intellectual content; and gave final approval of the version to be published.

Data Availability

The datasets created and/or analyzed during the current study are not publicly available, but are available from the corresponding author upon reasonable request.

REFERENCES

Abbass W, Aslam F, Ahmed M, Ahmed A, Alyousef R, Mohamed A (2023). Predicting the performance of existing pre-cast concrete pipes using destructive and non-destructive testing techniques. *Heliyon*, 9(4), e15471.

Angiulli G, Burrascano P, Ricci M, Versaci M (2024a). Advances in the integration of artificial intelligence and ultrasonic techniques for monitoring concrete structures: A comprehensive review. *Journal of Composites Science*, 8(12), 531.

Angiulli G, Calcagno S, La Foresta F, Versaci M (2024b). Concrete compressive strength prediction using combined non-destructive methods: A calibration procedure using preexisting conversion models based on Gaussian process regression. *Journal of Composites Science*, 8(8), 300.

Ansari MA, Ansari SS, Ghazi MS, Saqib M, Ibrahim SM, Saquib M (2024). Incorporating non-destructive UPV into machine learning models for predicting compressive strength in SCM concrete. *Materials Today: Proceedings*, 4, 59–67.

Asri Y, Benaicha M, Zaher M, Hafidi Alaoui A (2022). Prediction of the compressive strength of self-compacting concrete using artificial neural networks based on rheological parameters. *Structural Concrete*, 23(6), 3864–3876.

Asteris PG, Kolovos KG, Douvika MG, Roinos K (2016). Prediction of self-compacting concrete strength using artificial neural networks. *European Journal of Environmental and Civil Engineering*, 20(sup1), s102–s122.

Asteris PG, Skentou AD, Bardhan A, Samui P, Lourenço PB (2021). Soft computing techniques for the prediction of concrete compressive strength using non-destructive tests. *Construction and Building Materials*, 303, 124450.

Benaicha M (2024). AI-driven prediction of compressive strength in self-compacting concrete: Enhancing sustainability through ultrasonic measurements. *Sustainability*, 16(15), 6644.

Boccacci G, Frasca F, Bertolin C, Siani AM (2024). Diagnosis of historic reinforced concrete buildings: A literature review of non-destructive testing (NDT) techniques. *Procedia Structural Integrity*, 55, 160–167.

Chou J-S, Pham A-D (2015). Enhanced artificial intelligence for ensemble approach to predicting high performance concrete compressive strength. *Construction and Building Materials*, 49, 554–563.

Feng D-C, Liu Z-T, Wang X-D, Chen Y, Chang J-Q, Wei D-F, Jiang Z-M (2020). Machine learning-based compressive strength prediction for concrete: An adaptive boosting approach. *Construction and Building Materials*, 230, 117000.

Iqbal MF, Liu Q-F, Azim I, Zhu X, Yang J, Javed MF, Rauf M (2020). Prediction of mechanical properties of green concrete incorporating waste foundry sand based on gene expression programming. *Journal of Hazardous Materials*, 384, 121322.

Jibril MM, Zayyan MA, Malami SI, Usman AG, Salami BA, Rotimi A, Abba SI (2023). Implementation of nonlinear computing models and classical regression for predicting compressive strength of high-performance concrete. *Applied Engineering Sciences*, 15, 100133.

Kouddane B, Sbartaï ZM, Elachachi SM, Lamdouar N (2023). New multi-objective optimization to evaluate the compressive strength and variability of concrete by combining non-destructive techniques. *Journal of Building Engineering*, 77, 107526.

Lai MH, Wu KJ, Cheng X, Ho JCM, Wu JP, Chen JH, Zhang AJ (2022). Effect of fillers on the behaviour of heavy-weight concrete made by iron sand. *Construction and Building Materials*, 332, 127357.

Mirzaie Aliabadi M, Derakhshan Nezhad AH, Shahidzadeh MS, Dadpur A (2024). Date palm fibers to improve tensile strength in self-compacting concrete with silica fume. *Civil Engineering Infrastructures Journal,* In Press.

Moura MAN, Moreno AL, Ferreira GCS (2023). Ultrasonic testing on evaluation of concrete residual compressive strength: A review. *Construction and Building Materials*, 373, 130887.

Murty KSS, Rama Rao GV, Adiseshu S (2024). Experimental study on the effect of colloidal nano silica in self-compacting concrete containing ground granulated blast furnace slag. *Research on Engineering Structures and Materials*, 10(2), 1467–1481.

Pal A, Ahmed KS, Hossain FZ, Alam MS (2023). Machine learning models for predicting compressive strength of fiber-reinforced concrete containing waste rubber and recycled aggregate. *Journal of Cleaner Production*, 423, 138673.

Pazouki G, Tao Z, Saeed N, Kang W-H (2023). Using artificial intelligence methods to predict the compressive strength of concrete containing sugarcane bagasse ash. *Construction and Building Materials*, 409, 134047.

Ramkumar KB, Rajkumar KPR, Ahmmad SN, Murugesan J (2020). A review on performance of self-compacting concrete – Use of mineral admixtures and steel fibres with artificial neural network application. *Construction and Building Materials*, 261, 120215.

Roshan-Tabari, F., Toopchi-Nezhad, H., & Hashemi-Motlagh, G. (2024). Development and testing of a novel high-damping chlorobutyl rubber for structural viscoelastic damper devices. *Civil Engineering Infrastructures Journal*, 57(2), 337–355.

Reddy AN, Reddy GGK, Reddy PN, Reddy KS, Kavyateja BV (2024). Analyzing the impact of nano-sized silica on composite concrete: A static approach utilizing response surface method. *Research on Engineering Structures and Materials*, 10(2), 165–178.

Sadowski L, Nikoo M (2020). Non-destructive estimation of concrete compressive strength using ultrasonic pulse velocity and artificial neural network. *Measurement*, 152, 107328.

Sathiparan N, Jeyananthan P (2023). Prediction of masonry prism strength using machine learning technique: Effect of dimension and strength parameters. *Materials Today Communications*, 35, 106282.

Sathiparan N, Jeyananthan P, Subramaniam DN (2024). Surface response regression and machine learning techniques to predict the characteristics of pervious concrete using non-destructive meas-

urement: Ultrasonic pulse velocity and electrical resistivity. *Measurement*, 225, 114006.

Sayyar-Roudsari S, Shalbaftabar A, Damirchilo F, Taslimian R, Abu-Lebdeh T, Hamoush S, Yi S (2024). Defect classification of reinforced concrete structures with nondestructive tests using statistical and machine learning methods. *American Journal of Engineering and Applied Sciences*, 17(3), 102–115.

Shahidzadeh MS, Derakhshan Nezhad AH, Mirzaie Aliabadi M (2024a). Analyzing and examining the impact of various fiber types on the mechanical and functional characteristics of UHPC. *Research on Engineering Structures and Materials*, 11(3), 1219–1244.

Shahidzadeh MS, Mirzaie Aliabadi M, Mansouri Far H, Derakhshan Nezhad AH (2024b). Mechanical and rheological performance of plastic concrete: Investigation of several properties. *Research on Engineering Structures and Materials*, In Press.

Silva FAN, Delgado JMPQ, Cavalcanti RS, Azevedo AC, Guimarães AS, Lima AGB (2021). Use of nondestructive testing of ultrasound and artificial neural networks to estimate compressive strength of concrete. *Buildings*, 11(2), 44.

Wang L, Yi S, Yu Y, Gao C, Samali B (2024). Automated ultrasonic-based diagnosis of concrete compressive damage amidst temperature variations utilizing deep learning. *Mechanical Systems and Signal Processing*, 221, 111719.

Yang X, Yang H, Zhang S (2019). Rate-dependent constitutive models of S690 high- strength structural steel. *Construction and Building Materials,* 198(7), 597–607.

Yang H, Zhang JC, Du GF, Mao ZH (2021). Experimental study on the behavior of cross-shaped concrete-filled steel tubular intermediate long columns under axial compression. *Progress in Steel Building Structures*, 23(7), 49-57.

Yılmaz S, Özdemir E, Firat M, Ateş A (2022). Economic analysis and economic leakage level in water loss management and paths for future evaluation: A review. *Civil Engineering Infrastructures Journal*, 55(2), 195–209.

Yousef I, Al-Nawaiseh M, Al-Rawashdeh M (2024). Seismic assessment of base-isolated structure under a sequence of near-fault earthquake records. *Civil Engineering Infrastructures Journal*, 57(2), 267–285.

Zhang Y, Aslani F, Lehane B (2021a). Compressive strength of rubberized concrete: Regression and GA-BPNN approaches using ultrasonic pulse velocity. *Construction and Building Materials*, 307, 124951.

Zhang Y, Ma J, Zhang Y, Wang L (2021b). Prediction of compressive strength of high-performance concrete using machine learning algorithms. *Journal of Materials in Civil Engineering*, 33(10), 04021294.

Zheng Y, Lin Y, Ma S (2024). Axial compressive behavior of stiffened and multi-cell cross-shaped CFST stub columns. *Constructional Steel Research*, 213, 108399.

Zhu Y, Gardner L, Yang H (2023). Experimental investigation into the transverse impact performance of high-strength circular CFST members. *Thin-Walled Structures*, 189(3), 110923.